Electronic Supplementary Material (ESI) for ChemComm.

Supporting Information for

Construction of acid–base bifunctional covalent organic frameworks via Doebner reaction for catalysing cascade reaction

Xue-Tian Li,† Jie Zou,† Qi Yu, Yan Liu, Jing-Ru Li, Meng-Jing Li, Hui-Chao Ma, Gong-Jun Chen,* and Yu-Bin Dong*

Table of Contents

I. Instruments and methods (page S2)

II. Synthesis and characterization of model compound 2-(2-methoxyphenyl)quinoline-4-carboxylic acid via Doebner reaction (page S2, Fig. S1- Fig. S3)

III. Synthesis and characterization of COFs (page S4)

1. Synthesis and Characterization of TAPB-DMTP-PA-COF (Fig. S4- Fig. S15)

2. Synthesis and characterization of TAPB-TFPB-PA-COF (Fig. S16- Fig. S18)

3. Synthesis and characterization of TAPT-TFPB-PA-COF (Fig. S19- Fig. S21)

4. Synthesis and characterization of TAPB-TP-PA-COF (Fig. S22- Fig. S24)

5. Synthesis and characterization of TAPT-TP-PA-COF (Fig. S25- Fig. S27)

IV. Synthesis and characterization of benzylidenemalononitrile (page S24, Fig. S28-S30)

V. Leaching test (page S26, Fig. S31)

VI. Catalyst regeneration (page S27, Fig. S32)

VII. Comparison of TAPB-DMTP-PA-COF with the reported catalysts (page S29)

VIII. Control experiments for clarifying the cascade deacetalization−Knoevenagel condensation reaction process (page 30, Fig. S33-S37)

IX. Continuous flow-through operation (page S33, Fig. S38-S39)

X. Reference (page S35)

I. Instruments and methods

The reagents and solvents employed were commercially available and used without further purification. The powder diffractometer (XRD) patterns were collected by a D8 ADVANCEX-ray with Cu Kα radiation (λ = 1.5405 Å). The total surface areas of the COFs were measured by the BET (Brunauer–Emmer–Teller) method using N_2 adsorption at 77 K, this was done by the Micromeritics ASAP 2000 sorption/desorption analyzer. Infrared (IR) samples were prepared as KBr pellets, and spectra were obtained in the 400-4000cm^{-1} range using a Perkin-Elmer 1600 FTIR spectrometer. ^{13}C NMR spectra were recorded on a MERCURY plus 400 spectrometer operating at resonance frequencies of 400 MHz. Thermogravimetric analyses (TGA) were carried out under flowing nitrogen at a heating rate of 10 °C·min^{-1} on a TA Instrument Q5 analyzer. XPS spectra were obtained from PHI Versaprobe II. TEM (transmission electron microscopy) analysis was performed on a JEOL 2100 Electron Microscope at an operating voltage of 200 kV. Scanning electron microscopy (SEM) images were taken on a SUB010 scanning electron microscope with acceleration voltage of 20 kV.

II. Synthesis and characterization of model compound 2-(2-methoxyphenyl)quinoline-4-carboxylic acid via Doebner reaction

Synthesis of 2-(2-methoxy-phenyl)-quinoline-4-carboxylic acid. A mixture of 2-methoxybenzaldehyde (120.8 μL, 1.0 mmol), benzenamine (91.3 μL, 1.0 mmol), pyruvic acid (75.0 μL, 1.5 mmol) and 2, 3-dichloro-5,6-dicyano-1,4-benzoquinone (DDQ) (50 mg, 1.0 mmol) in 5 mL ethanol was refluxed for 3 h (monitored by TLC). Then, the reaction mixture poured into ice water (10 mL) and the obtained crude product was purified by column chromatography. The product was characterizated by MS, ^{1}H NMR, and FT-IR spectra.

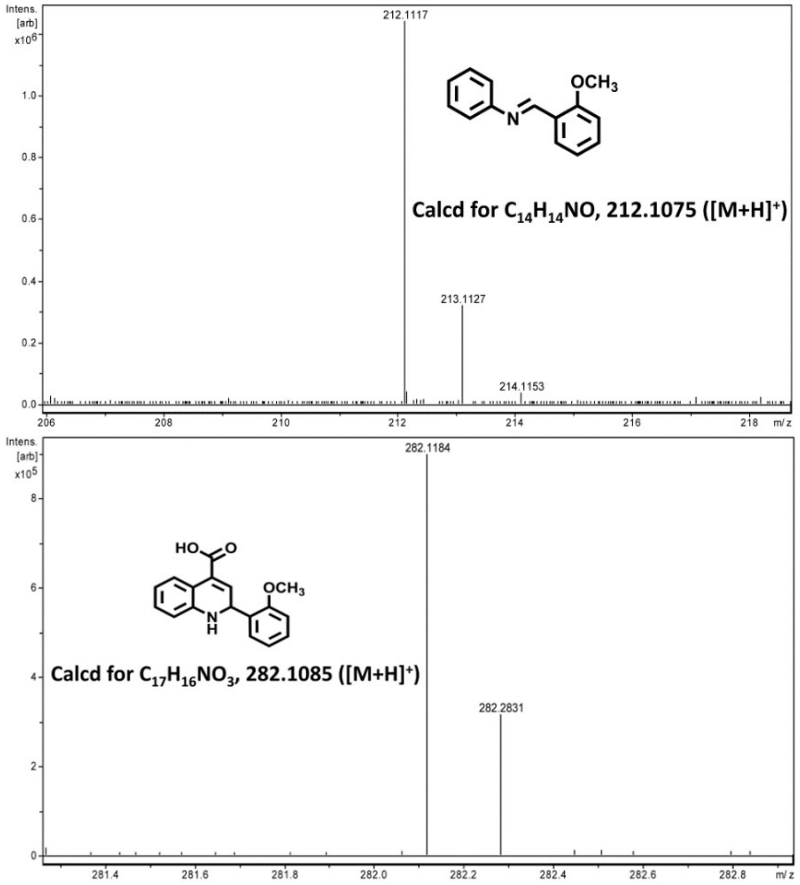

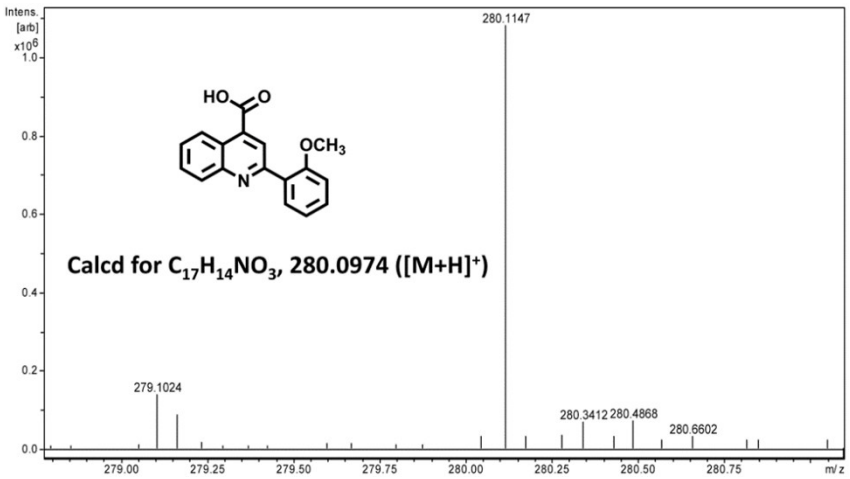

Fig. S1 ESI-MS spectra of 2-(2-methoxy-phenyl)-quinoline-4-carboxylic acid, and its intermediates from the reaction of aniline, 2-methoxybenzaldehyde and pyruvic acid

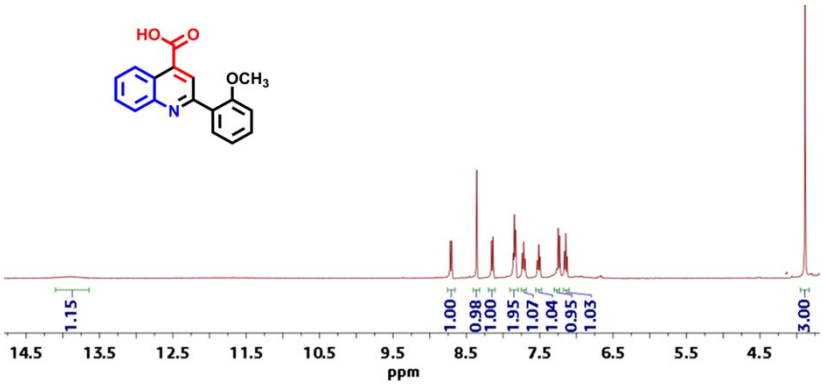

Fig. S2 ^{1}H NMR of 2-(2-methoxyphenyl)-1, 2-dihydroquinoline-4-carboxylic acid.

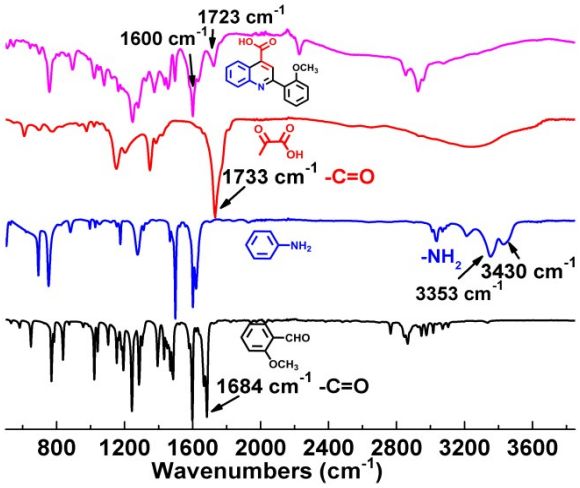

Fig. S3 FT-IR spectra of 2-(2-methoxyphenyl)-1, 2-dihydroquinoline-4-carboxylic acid and its starting materials.

III. Synthesis and characterization of COFs

1. Synthesis and Characterization of TAPB-DMTP-PA-COF.

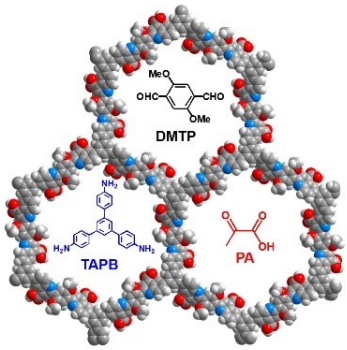

TAPB-DMTP-PA-COF

A mixture of 1,3,5-tri(4-aminophenyl)benzene (TAPB) (0.040 mmol, 14.0 mg), 2,5-dimethoxy terephthalaldehyde (DMTP) (0.060 mmol, 11.7 mg), pyruvic acid (PA) (0.12 mmol, 12 μL,), 2,3-dichloro-5,6-dicyano-1,4-benzoquinone (DDQ) (10.67 mg, 0.04 mmol) and in the *o*-dichlorobenzene (*o*-DCB)/*n*-BuOH (1.0/1.0 mL) mixture was sealed in a Pyrex tube (35 mL) and heated under N_2 at 120 °C for 3 days. The generated solids were collected by centrifugation and completely washed with dichloromethane and ethanol and dried in vacuum to afford **TAPB-DMTP-PA-COF** in 85 % yield.

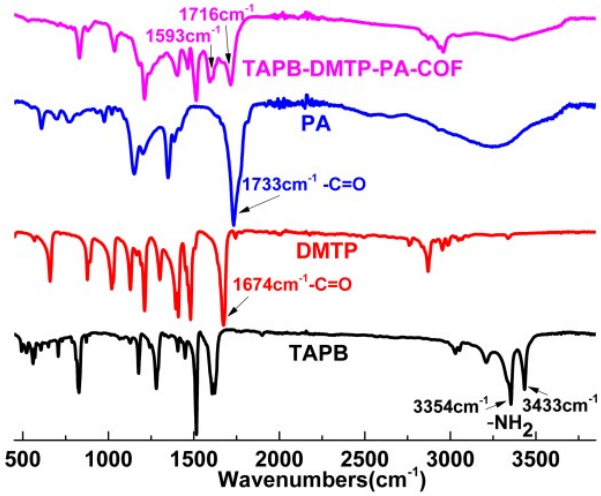

Fig. S4 FT-IR spectra of **TAPB-DMTP-PA-COF** and its monomers. The disappearance of the peaks at 3354 cm^{-1}, 3433 cm^{-1} (N-H band for TAPB), 1674 cm^{-1} (C=O band for DMTP) and 1733 cm^{-1} (C=O band for PA) and the appearance of characteristic bands at 1593cm^{-1} and 1716cm^{-1} associated with pyridyl stretching band and C=O band of carboxylic acids demonstrated the successful formation of **TAPB-DMTP-PA-COF**.

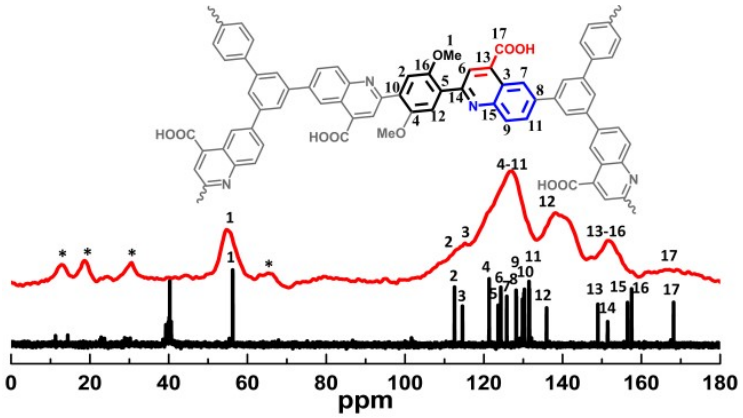

Fig. S5 ^{13}C NMR spectrum of **TAPB-DMTP-PA-COF** (red line) and ^{13}C NMR spectrum of model compound (2-(2-methoxyphenyl)-1,2-dihydroquinoline-4-carboxylic acid) (black line). The existence of methoxy (56.5 ppm), aromatic (100-155 ppm) and carboxylic acid (167.5 ppm) carbons was well supported the formation of **TAPB-DMTP-PA-COF** (the asterisks denote the solvent *n*-butyl alcohol).

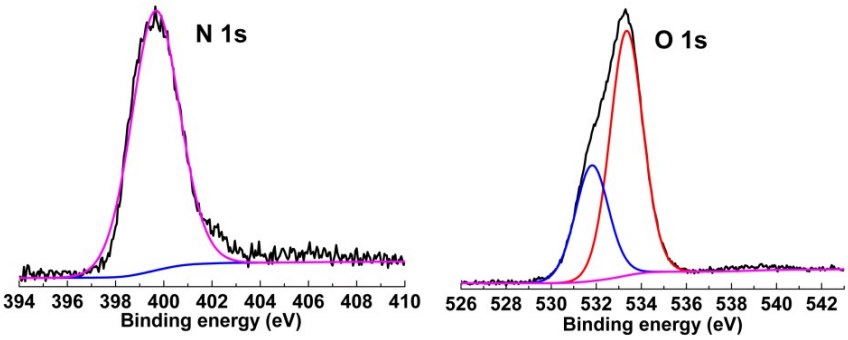

Fig. S6 XPS spectra of **TAPB-DMTP-PA-COF**. The N 1s peak at 399.7 eV originated from quinolyl group, and O 1s peaks at 531.7 and 533.3 eV respectively associated with methoxyl and carboxyl moieties were observed.

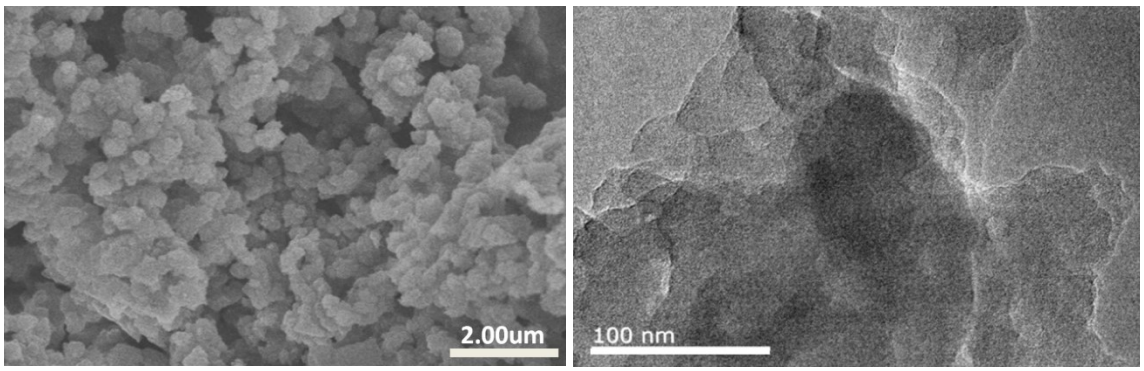

Fig. S7 SEM (left) and TEM (right) images of **TAPB-DMTP-PA-COF**.

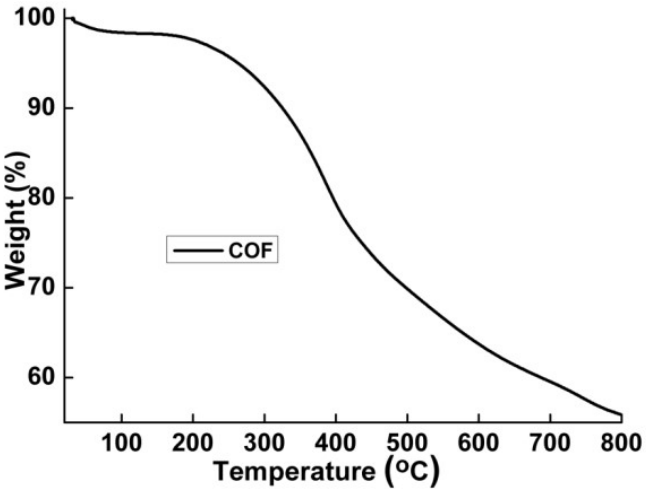

Fig. S8 TGA trace of **TAPB-DMTP-PA-COF**.

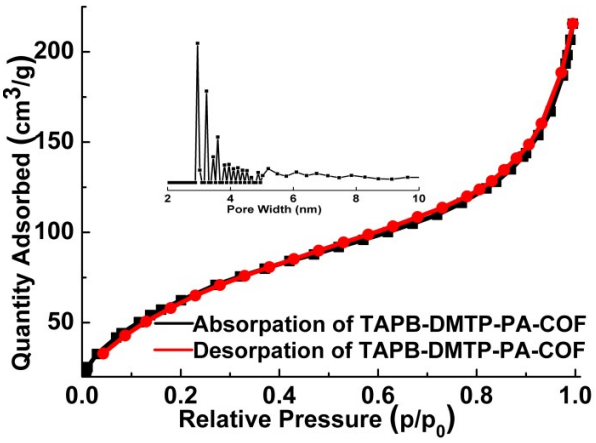

Fig. S9 N_2 adsorption and desorption isotherms of **TAPB-DMTP-PA-COF**. Its pore size distribution is shown as inset.

Structural modeling of **TAPB-DMTP-PA-COF** was generated using the Materials Studio (ver. 2018) suite of programs. Molecular geometry optimization was performed with MS DMol3 module. The initial lattice was created by starting with the space group *P*6. The *a* and *b* lattice parameters (initially 37.2204 Å) were estimated according to the center to center distance between the vertices of COF. The constructed model was geometry optimized using the Forcite module (Universal force fields, Ewald summations). Then the calculated PXRD pattern was generated with the Reflex Plus module. Finally, Pawley refinement was applied for profile fitting, producing the refined PXRD profile with the lattice parameters of $a = b = 37.2204$ Å (± 0.002) Å and $c = 3.8725$ (± 0.002) Å. *R*wp and *R*p values converged to 6.18 and 4.72 %, respectively. Reflex Module in Material Studio using data from $2\theta = 2.0\text{-}30°$. Backgrounds were first refined applying a 2nd order Chebyschev Polynomial.

Atomistic coordinates for the AA-stacking mode of **TAPB-DMTP-PA-COF** (space group *P*6, $a = b = 37.2204$ Å, $c = 3.8725$ Å, $\alpha = \beta = 90°$ and $\gamma = 120°$, w*R*p = 6.18 % and *R*p = 4.72 %).

Table S1. Simulated AA-stacking structure of **TAPB-DMTP-PA-COF**

Atom	x/a	y/b	z/c	Atom	x/a	y/b	z/c
C1	0.35755	0.64709	0.65748	C2	0.37659	0.69057	0.65743
C3	0.38302	0.62634	0.66173	C4	0.36883	0.58786	0.49597
C5	0.39158	0.56690	0.51176	C6	0.43084	0.58698	0.67498
C7	0.44543	0.62548	0.83340	C8	0.42152	0.64470	0.83228
N9	0.45475	0.56897	0.68009	C10	0.44291	0.53172	0.52967
C11	0.47150	0.51462	0.54367	C12	0.45681	0.47165	0.57003
C13	0.48557	0.45755	0.55146	O14	0.41403	0.44454	0.62614
C15	0.40091	0.40389	0.75508	H16	0.41005	0.70907	0.65860
H17	0.34117	0.57573	0.34059	C18	0.37765	0.52732	0.36029
H19	0.47514	0.64030	0.96408	H20	0.43305	0.67363	0.97104
C21	0.40451	0.51098	0.35962	H22	0.47472	0.42466	0.54543
H23	0.41917	0.40550	0.98657	H24	0.40384	0.38427	0.55443
H25	0.36775	0.38913	0.82944	H26	0.39530	0.48206	0.22737
C27	0.66490	0.49904	0.21921	O28	0.67110	0.52490	-0.00171
O29	0.69843	0.49669	0.35399	H30	0.72569	0.51679	0.23913

Table S2. Simulated AB-stacking structure of **TAPB-DMTP-PA-COF**

Atom	x/a	y/b	z/c	Atom	x/a	y/b	z/c
C1	-0.30974	0.31241	0.49438	C2	-0.28930	0.35666	0.49594
C3	-0.28622	0.29186	0.48198	C4	-0.29180	0.26581	0.33913
C5	-0.26709	0.24655	0.31565	C6	-0.23807	0.25200	0.44771
C7	-0.23272	0.27722	0.59205	C8	-0.25623	0.29753	0.60776
N9	-0.21486	0.23289	0.43546	C10	-0.21668	0.20847	0.30127
C11	-0.19043	0.19057	0.30046	C12	-0.20412	0.14933	0.24110
C13	-0.17495	0.13524	0.22737	O14	-0.24551	0.12396	0.20134
C15	-0.26731	0.08161	0.14043	H16	-0.25719	0.37371	0.49469
H17	-0.31419	0.26128	0.25082	C18	-0.26963	0.22203	0.16940
H19	-0.21159	0.28110	0.68577	H20	-0.25148	0.31627	0.71226
C21	-0.24409	0.20337	0.16451	H22	-0.18568	0.10566	0.18232
H23	-0.26447	0.06082	0.23242	H24	-0.25490	0.07938	0.01616
H25	-0.30038	0.07182	0.12536	H26	-0.29559	0.21584	0.02613
C27	-0.29929	0.24736	-0.04467	O28	-0.31550	0.18076	-0.04533
H29	-0.24477	0.18656	0.05848	C30	-0.02468	0.02086	0.20892
C31	-0.04326	-0.02341	0.20816	C32	-0.04911	0.04153	0.20833
C33	-0.03115	0.08499	0.24697	C34	-0.05254	0.10777	0.22853

C35	-0.09652	0.08396	0.20607	C36	-0.11640	0.04076	0.17417
C37	-0.09270	0.02054	0.16854	N38	-0.11978	0.10289	0.22077
C39	-0.10411	0.14469	0.24501	C40	-0.13217	0.16018	0.27458
C41	-0.12034	0.19926	0.35559	C42	-0.14886	0.21435	0.36182
O43	-0.08184	0.22147	0.43125	C44	-0.06289	0.26042	0.52268
H45	-0.07481	-0.04037	0.20596	H46	-0.00145	0.10123	0.29272
C47	-0.03309	0.15247	0.23381	H48	-0.14809	0.02388	0.15458
H49	-0.10889	-0.01028	0.13510	C50	-0.05990	0.16989	0.23518
H51	-0.13898	0.24347	0.41203	H52	-0.08153	0.25803	0.63555
H53	-0.05993	0.28560	0.43945	H54	-0.03171	0.26774	0.56445
C55	0.01117	0.18028	0.23339	C56	0.03854	0.17289	0.12955
C57	0.08231	0.19937	0.13591	C58	0.09979	0.23589	0.23592
C59	0.07336	0.24514	0.33297	C60	0.02985	0.21722	0.33545
H61	-0.04686	0.20163	0.22691	H62	0.02692	0.14781	0.04812
H63	0.10151	0.19226	0.06716	H64	0.13152	0.25568	0.23765
H65	0.08585	0.27218	0.40212	H66	0.01197	0.22435	0.41364
H67	0.44039	0.71616	0.50285				

Atomistic coordinates for the AB-stacking mode of **TAPB-DMTP-PA-COF** (space group *P*63, $a = b =$ 36.8357 Å, c = 7.7843 Å, $\alpha = \beta = 90°$ and $\gamma = 120°$, w*R*p = 10.07 % and *R*p = 7.77 %).

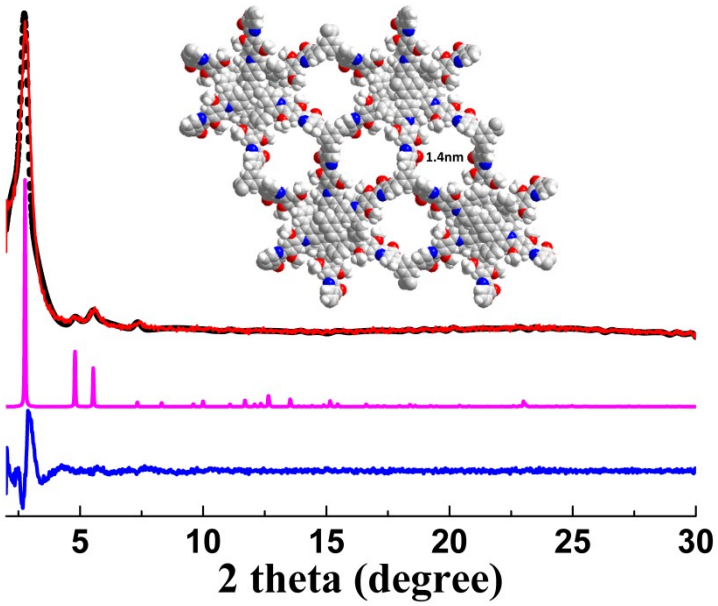

Fig. 10 Powder X-ray diffraction patterns of **TAPB-DMTP-PA-COF**: comparison between the experimental (red line) and Pawley refined (black dots) profiles, the simulated pattern for eclipsed (AB) stacking mode (pink line) and the refinement difference (blue line). Inset is AB-stacking structure of **TAPB-DMTP-PA-COF**.

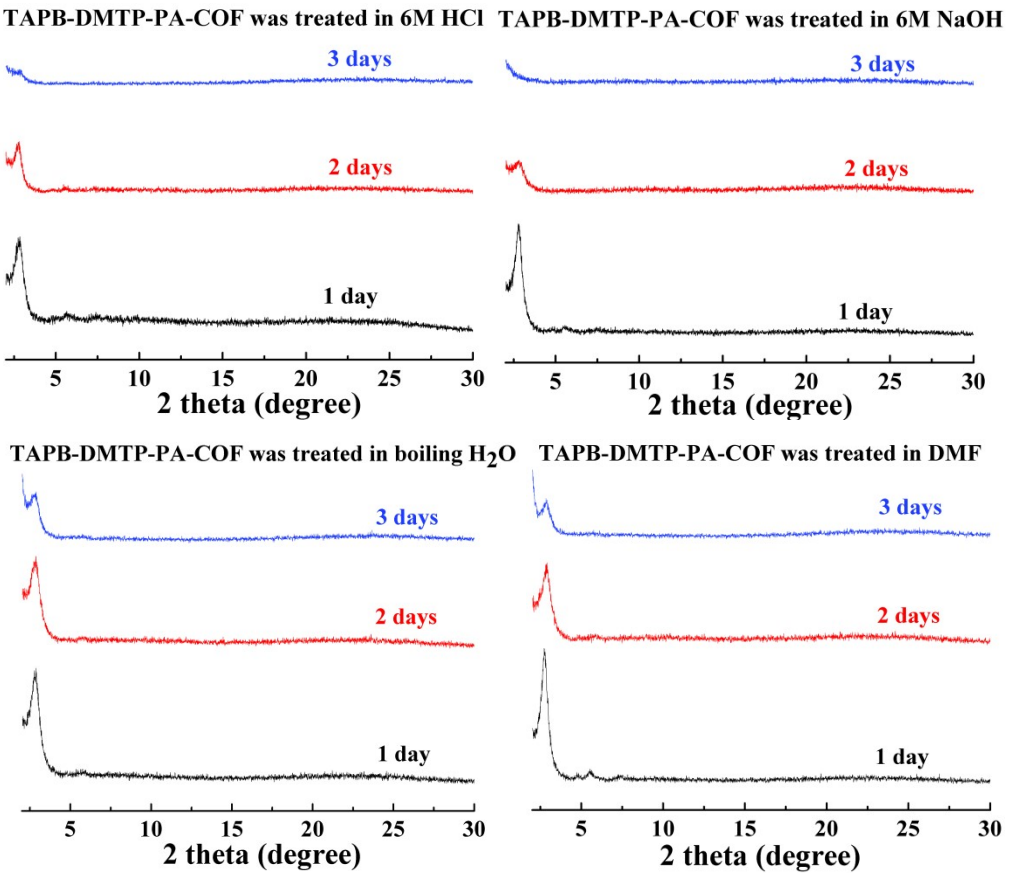

Fig. S11 PXRD patterns of **TAPB-DMTP-PA-COF** treated in different solvents. **TAPB-DMTP-PA-COF** treated in boiling H_2O and 6M NaOH showed no obvious weight loss for 3 days, but there is ca. 5.0 % weight loss was observed after it was treated in DMF and 6M HCl for 3 days.

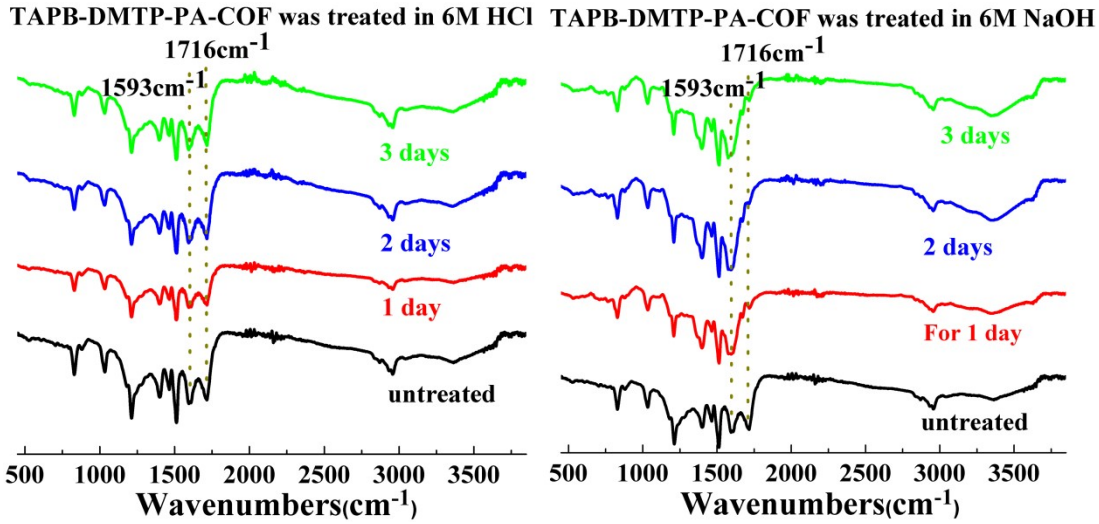

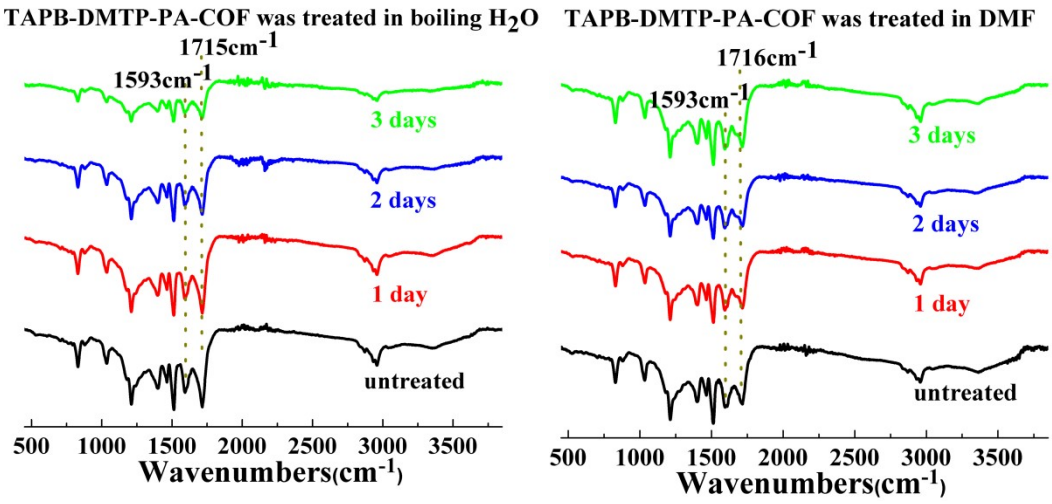

Fig. S12 FT-IR spectra of **TAPB-DMTP-PA-COF** treated in different solvents.

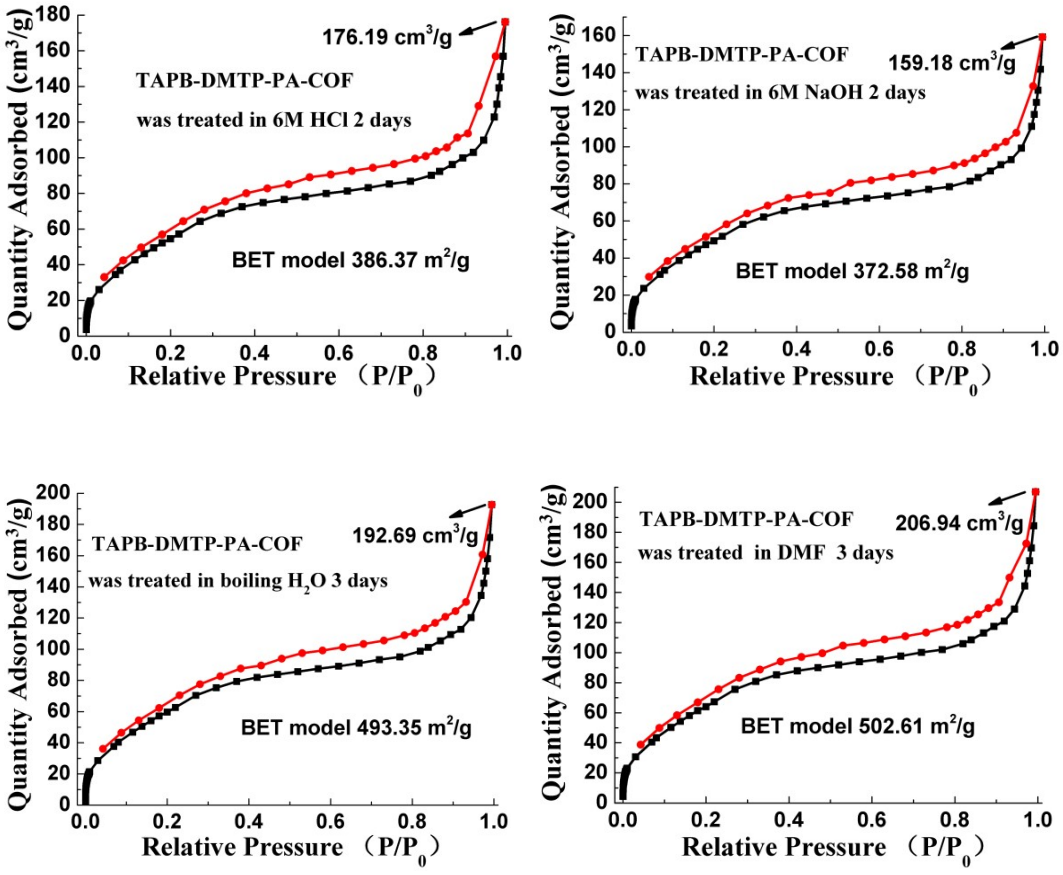

Fig. S13 N_2 adsorption and desorption isotherms of **TAPB-DMTP-PA-COF** treated in different solvents (boiling H_2O and DMF for 3 days, 6M HCl and 6M NaOH for 2 days). The slightly decreased adsorption capacity might result from the decreased crystallinity of **TAPB-DMTP-PA-COF** after treatment.

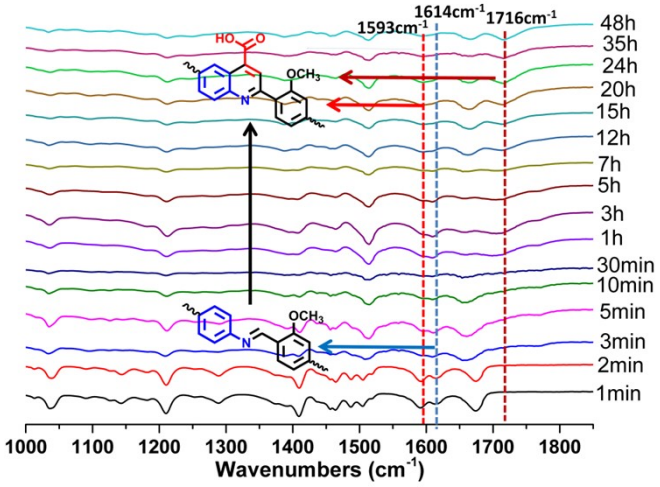

Fig. S14 FT-IR spectra for monitoring the formation of **TAPB-DMTP-PA-COF**. A mixture of 1,3,5-tri(4-aminophenyl)benzene (TAPB) (0.040 mmol, 14.0 mg), 2,5-dimethoxy terephthalaldehyde (DMTP) (0.060 mmol, 11.7 mg), pyruvic acid (PA) (0.12 mmol, 12 μL), 2,3-dichloro-5,6-dicyano-1,4-benzoquinone (DDQ) (10.67 mg, 0.04 mmol) in *o*-dichlorobenzene (*o*-DCB)/*n*-BuOH (1.0/1.0 mL) was sealed in a Pyrex tube (35 mL) and heated in N_2 at 120 °C. The generated solids were collected by centrifugation at different time, and they were completely washed with dichloromethane and ethanol and dried in vacuum for IR measurement.

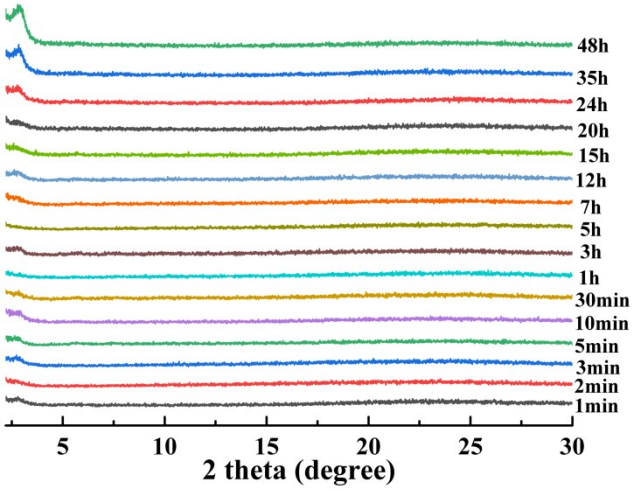

Fig. S15 PXRD spectra for monitoring the **TAPB-DMTP-PA-COF** formation.

2. Synthesis and characterization of TAPB-TFPB-PA-COF

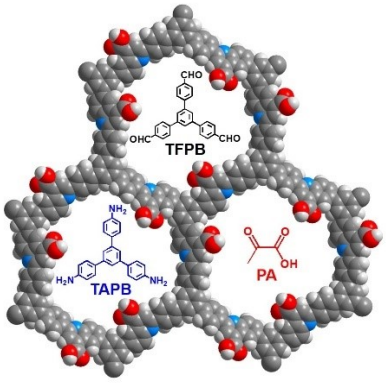

TAPB-TFPB-PA-COF

TAPB-TFPB-PA-COF was obtained by combination of TAPB, TFPB and PA via Doebner reaction. The synthesis procedure is the same as that of **TAPB-DMTP-PA-COF**. Yield, 88 %.

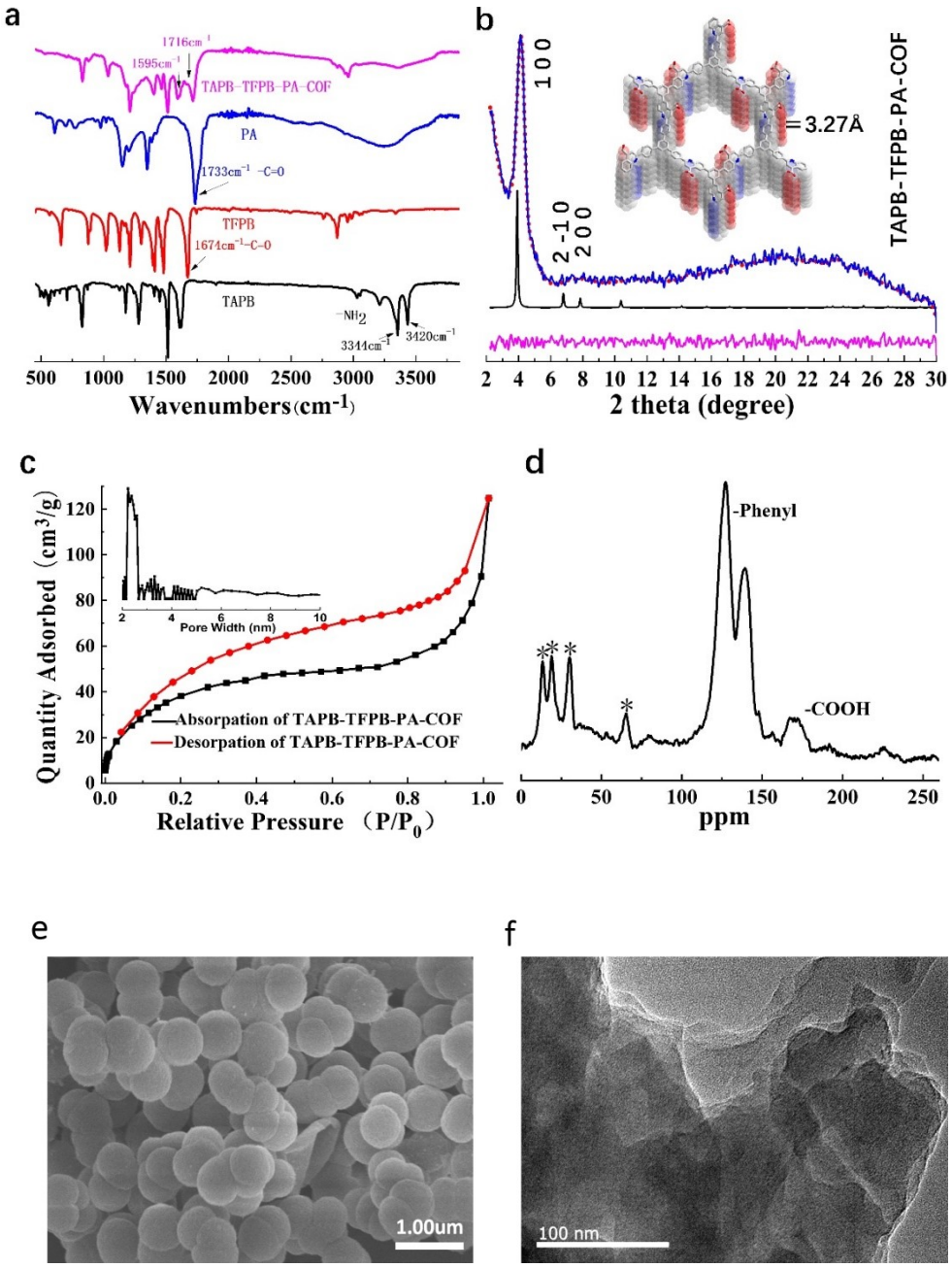

Fig. S16 a) FT-IR spectra of **TAPB-TFPB-PA-COF** and its monomers. The characteristic peaks of amine (3344 and 3420 cm^{-1}), aldehyde (1674 cm^{-1}) and C=O of pyruvic acid (1733 cm^{-1}) disappeared after reaction, meanwhile the characteristic peaks at 1595 and 1716 cm^{-1} appeared, demonstrating the formation of **TAPB-TFPB-PA-COF**. b) PXRD of **TAPB-TFPB-PA-COF**: comparison between the experimental (blue line) and Pawley refined (red dots) profiles, the simulated pattern for eclipsed (AA) stacking mode (black line) and the refinement difference (purple line). Inset is the simulated structure of **TAPB-TFPB-PA-COF**. c) N_2 adsorption at 77 K revealed absorption amount of **TAPB-TFPB-PA-COF** is 109.81 cm^3/g, and its surface area calculated based on the BET model was determined as 165.37 m^2/g. Pore size distribution curve, calculated from Barrett-Joyner-Halenda analysisa, showed that the pore width of **TAPB-TFPB-PA-COF** is centered at 2.2 nm, which is in good agreement with its simulated structure. d) ^{13}C (CP/MAS) NMR

spectrum. The peaks at 109-160 ppm and 170 ppm are respectively associated with aromatic and carboxylic acid carbons, and the asterisks denote the solvent *n*-butyl alcohol. e) TEM image of **TAPB-TFPB-PA-COF**. f) SEM image of **TAPB-TFPB-PA-COF**.

The simulation method is the same as that of **TAPB-DMTP-PA-COF**. Atomistic coordinates for the AA-stacking mode of **TAPB-TFPB-PA-COF** (space group *P*3, $a = b = 26.0294$ Å, $c = 3.8304$ Å, $\alpha = \beta = 90°$ and $\gamma = 120°$, w*R*p = 3.29 % and *R*p = 2.45 %).

Table S3. Simulated structure of **TAPB-TFPB-PA-COF**

Atom	x/a	y/b	z/c	Atom	x/a	y/b	z/c
C1	2.26186	2.81845	0.32877	C2	2.29250	2.78726	0.31658
C3	2.26910	2.73147	0.47806	C4	2.21369	2.70738	0.64655
C5	2.18038	2.73666	0.64057	C6	2.20642	2.79372	0.48874
C7	2.30214	2.69823	0.47216	C8	2.27140	2.63585	0.47087
C9	3.10113	3.22745	0.47110	C10	3.06334	3.16603	0.46276
C11	3.07932	3.12778	0.62734	C12	3.13447	3.15291	0.79798
C13	3.17263	3.21431	0.80311	C14	3.15657	3.25285	0.63985
C15	3.03859	3.06216	0.62342	C16	2.97674	3.03809	0.62304
H17	2.28050	2.86160	0.20613	H18	2.33401	2.80661	0.17463
H19	2.19849	2.66719	0.79474	H20	2.22348	2.61199	0.47039
H21	3.08731	3.25525	0.33792	H22	3.02235	3.14862	0.31737
H23	3.14751	3.12534	0.94016	H24	3.21352	3.23056	0.94610
H25	2.95875	3.06753	0.62370	N26	0.64737	0.82210	0.49671
C27	0.68102	0.87650	0.64323	C28	0.65211	0.90494	0.78678
C29	0.58978	0.87738	0.78656	H30	0.67703	0.94898	0.89431
C31	0.56294	0.91184	0.93215	O32	0.59380	0.95619	1.15832
O33	0.51404	0.90221	0.84303	H34	0.57500	0.97712	1.25334

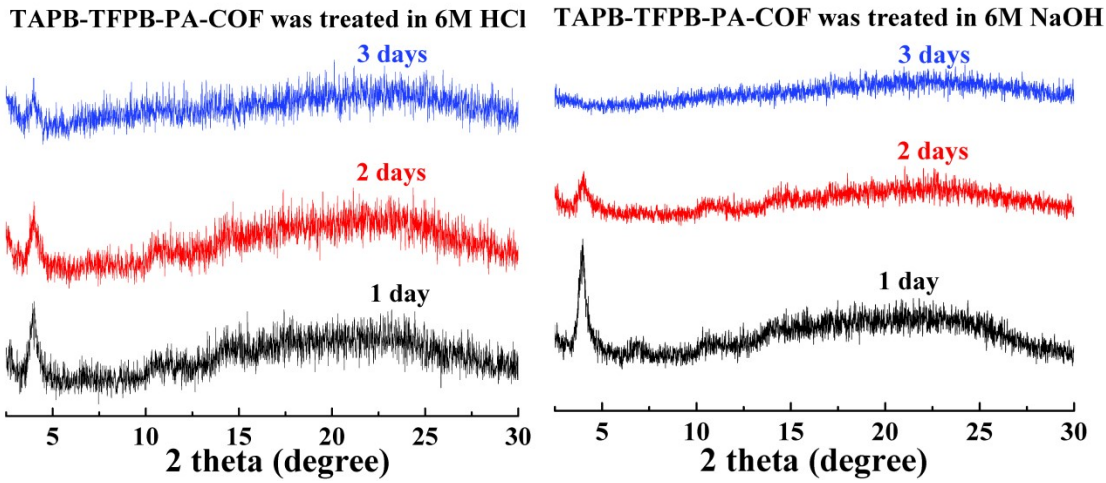

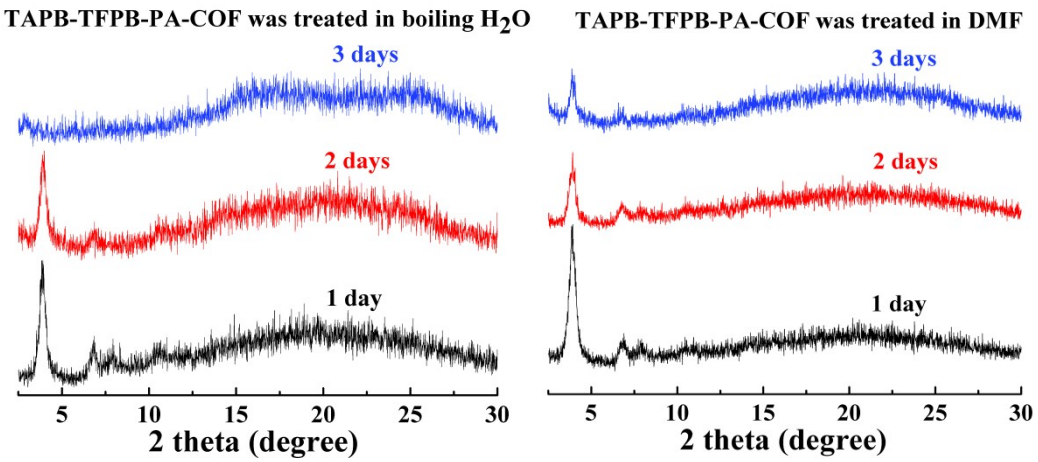

Fig. S17 PXRD patterns of **TAPB-TFPB-PA-COF** treated in different solvents. No obvious weight loss for **TAPB-TFPB-PA-COF** was observed in boiling H_2O and 6M NaOH, but there is about 4.8 % weight loss in DMF and 6M HCl after treatment.

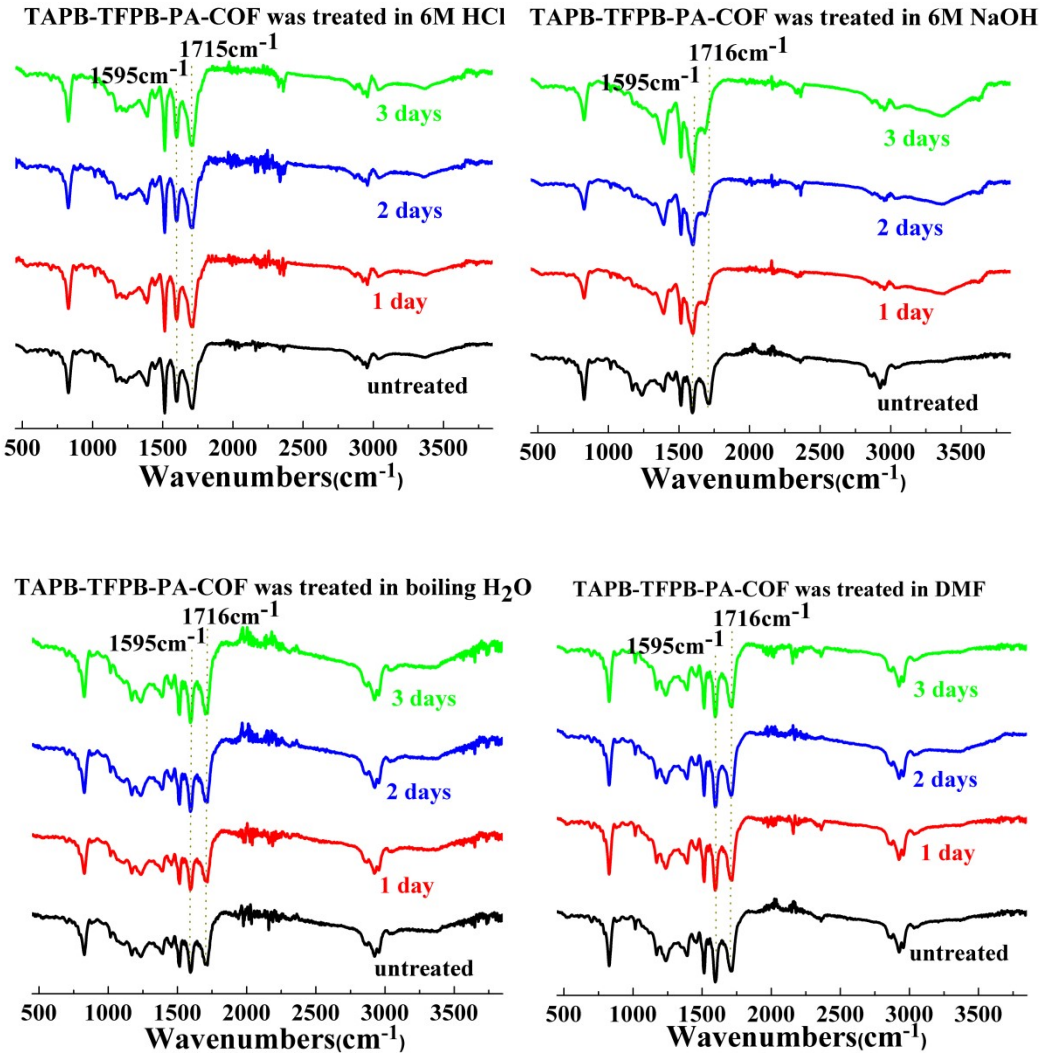

Fig. S18 FT-IR spectra of **TAPB-TFPB-PA-COF** treated in different solvents.

3. Synthesis and characterization of TAPT-TFPB-PA-COF

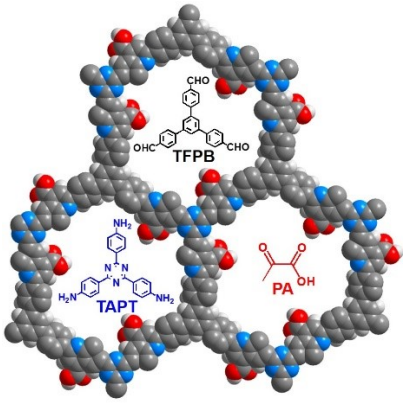

TAPT-TFPB-PA-COF

TAPT-TFPB-PA-COF was obtained by combination of TAPT, TFPB and PA via Doebner reaction. The synthesis procedure is the same as that of **TAPB-DMTP-PA-COF**. Yield, 89 %.

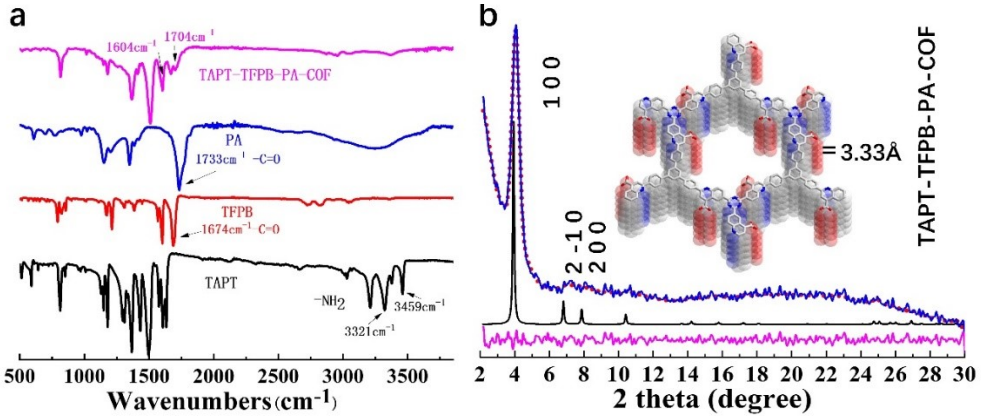

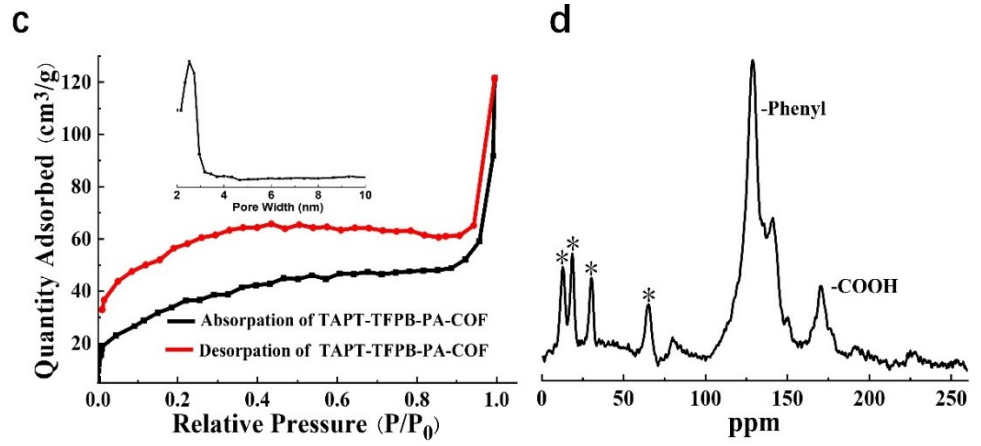

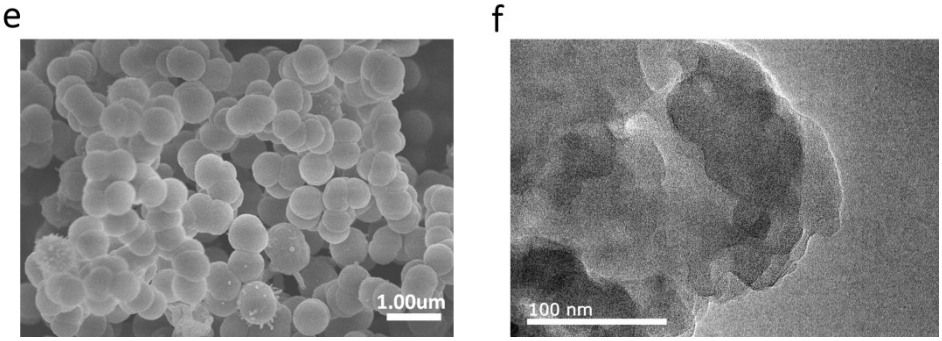

Fig. S19 a) FT-IR spectra of **TAPT-TFPB-PA-COF** and its monomers. The characteristic peaks of amine (3321 and 3459 cm^{-1}), aldehyde (1674 cm^{-1}) and C=O of pyruvic acid (1733 cm^{-1}) disappeared after reaction, meanwhile the characteristic peaks at 1604 and 1704 cm^{-1} appeared, demonstrating the formation of **TAPT-TFPB-PA-COF**. b) PXRD of **TAPT-TFPB-PA-COF**: comparison between the experimental (blue line) and Pawley refined (red dots) profiles, the simulated patterns for eclipsed (AA) stacking mode (black line) and the refinement difference (purple line). Inset is the simulated structure of **TAPT-TFPB-PA-COF**. c) N_2 adsorption at 77 K revealed absorption amount of **TAPT-TFPB-PA-COF** is 121.56 cm^3/g, and its surface area calculated based on the BET model was determined as 125.58 m^2/g. Pore size distribution curve, calculated from Barrett-Joyner-Halenda analysis, showed that the pore width of **TAPT-TFPB-PA-COF** is centered at 2.1 nm, which is in good agreement with its simulated structure. d) ^{13}C (CP/MAS) NMR spectrum. The peaks at 109-160 ppm and 170 ppm are respectively associated with aromatic and carboxylic acid carbons, the asterisks denote the solvent *n*-butyl alcohol. e) TEM image of **TAPT-TFPB-PA-COF**. f) SEM image of **TAPT-TFPB-PA-COF**.

The simulation method is the same as that of **TAPB-DMTP-PA-COF**. Atomistic coordinates for the AA-stacking mode of **TATP-TFPB-PA-COF** (space group *P*3, $a = b = 25.9242$ Å, $c = 3.5944$ Å, $\alpha = \beta = 90°$ and $\gamma = 120°$, w*R*p = 3.95 % and *R*p = 2.85 %).

Table S4. Simulated structure of **TAPT-TFPB-PA-COF**

Atom	x/a	y/b	z/c	Atom	x/a	y/b	z/c
C1	2.27573	2.82796	0.79349	C2	2.30507	2.79524	0.80859
C3	2.27350	2.73333	0.75241	C4	2.21206	2.70485	0.67616
C5	2.18233	2.73778	0.64403	C6	2.21497	2.79982	0.71422
C7	2.30469	2.69854	0.76692	N8	2.27323	2.63821	0.76644
C9	3.09521	3.22889	0.49599	C10	3.05834	3.16703	0.48826
C11	3.07769	3.12914	0.63613	C12	3.13573	3.15563	0.78589
C13	3.17325	3.21740	0.78125	C14	3.15318	3.25460	0.63791
C15	3.03775	3.06275	0.63523	C16	2.97541	3.03712	0.63512
H17	2.30007	2.87545	0.84501	H18	2.35239	2.81808	0.87003
H19	2.18807	2.65691	0.64835	H20	3.07942	3.25700	0.37848
H21	3.01546	3.14933	0.35455	H22	3.15193	3.12917	0.91995
H23	3.21714	3.23623	0.90422	H24	2.95644	3.06575	0.63520
N25	0.64517	0.81250	0.70810	C26	0.67987	0.87165	0.63979
C27	0.65298	0.90564	0.56140	C28	0.59061	0.87905	0.55197
H29	0.68049	0.95230	0.49086	C30	0.56539	0.91663	0.42565
O31	0.59806	0.97615	0.45123	O32	0.51716	0.89490	0.27216
H33	0.58169	0.99951	0.35109				

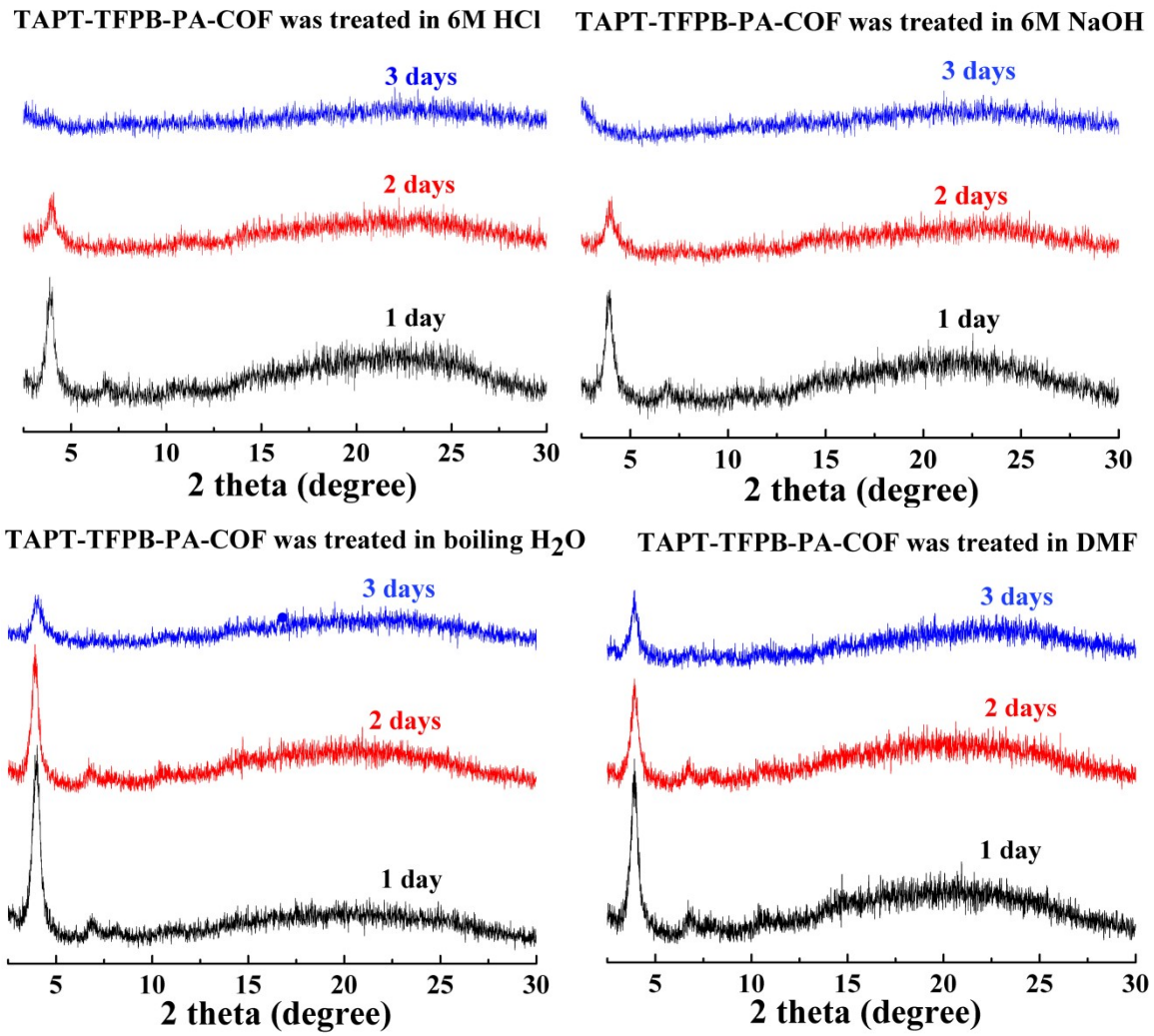

Fig. S20 PXRD patterns of **TAPT-TFPB-PA-COF** treated in different solvents. No obvious weight loss for **TAPT-TFPB-PA-COF** treated by boiling H_2O and 6M NaOH was observed, but there is about 5.5 % weight loss in DMF and 6M HCl after treatment.

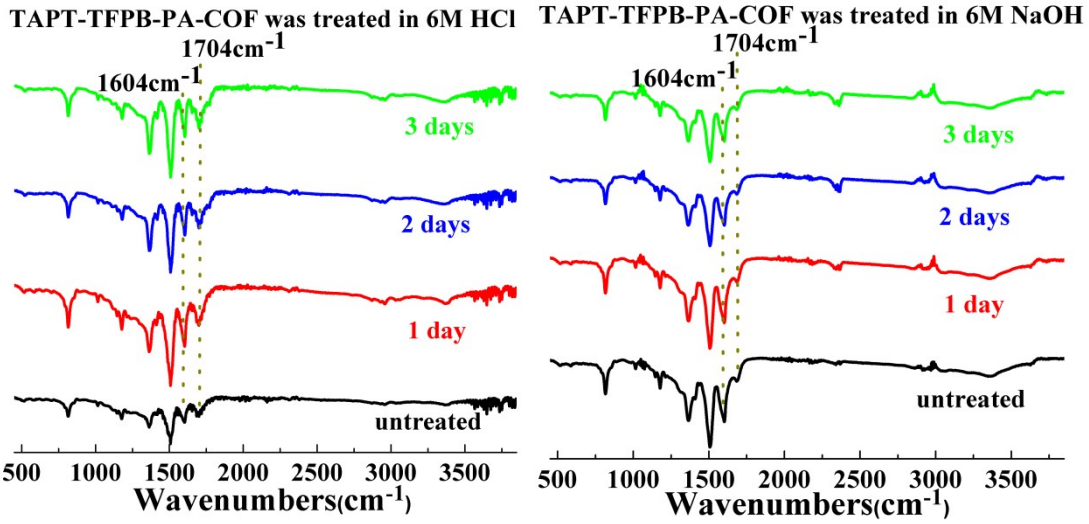

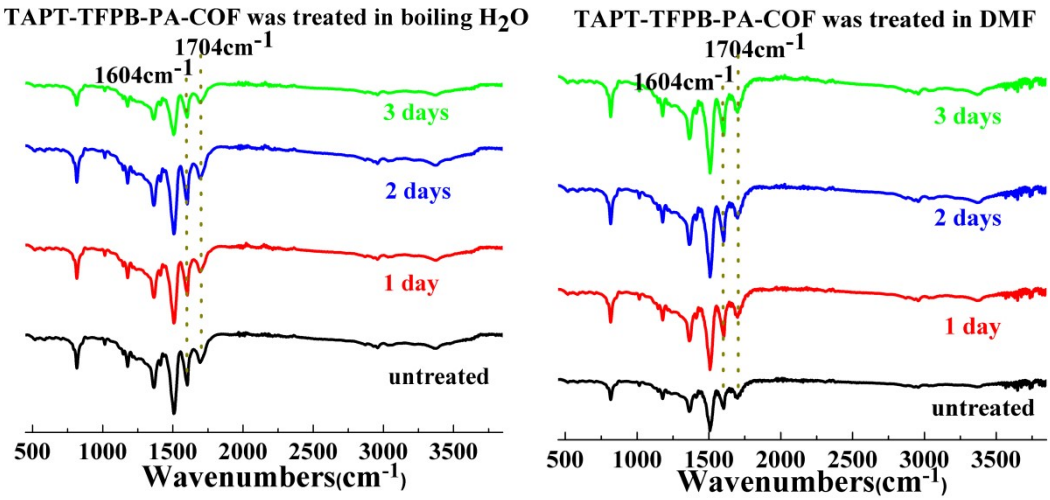

Fig. S21 FT-IR spectra of **TAPT-TFPB-PA-COF** treated in different solvents.

4. Synthesis and characterization of TAPB-TP-PA-COF

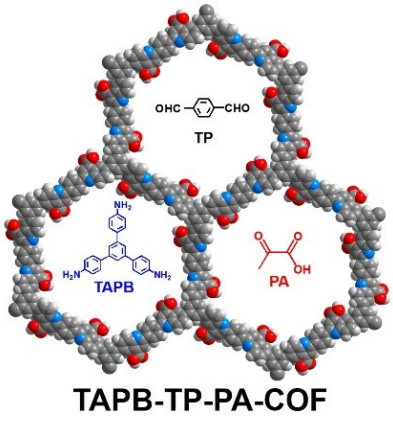

TAPB-TP-PA-COF was obtained by combination of TATP, TFPB and PA via Doebner reaction. The synthesis procedure is the same as that of **TAPB-DMTP-PA-COF**. Yield, 85 %.

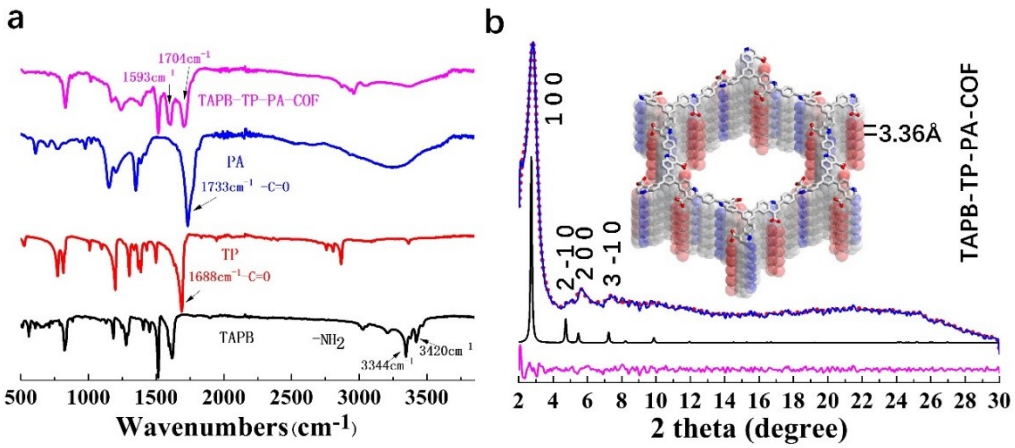

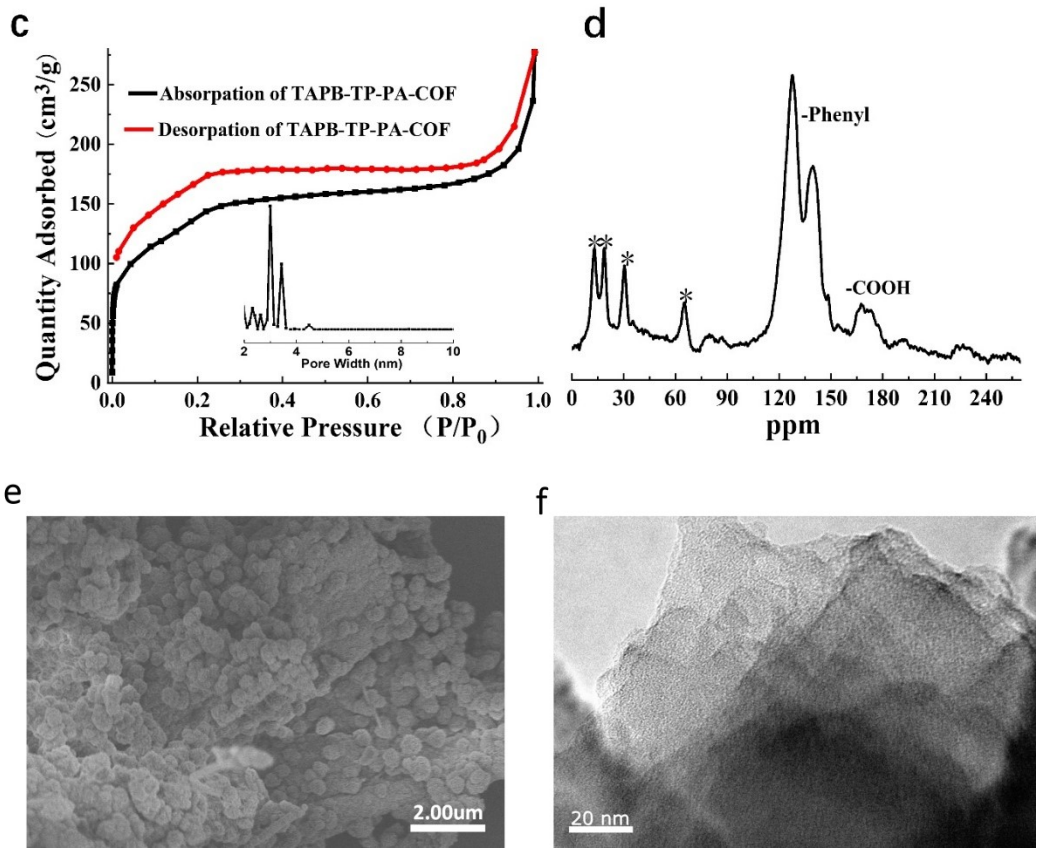

Fig. S22 a) FT-IR spectra of **TAPB-TP-PA-COF** and its monomers. The characteristic peaks of amine (3344 and 3420 cm^{-1}), aldehyde (1688 cm^{-1}) and C=O of pyruvic acid (1733 cm^{-1}) in the monomers disappeared after reaction, meanwhile the characteristic peaks at 1593 and 1704 cm^{-1} appeared, demonstrating the formation of **TAPB-TP-PA-COF**. b) PXRD of **TAPB-TP-PA-COF**: comparison between the experimental (blue line) and Pawley refined (red dots) profiles, the simulated patterns for eclipsed (AA) stacking mode (black line) and the refinement difference (purple line). Inset is the simulated structure of **TAPB-TP-PA-COF**. c) N_2 adsorption at 77 K revealed absorption amount of **TAPB-TP-PA-COF** is 277.07 cm^3/g, and its surface area calculated on basis of the BET model was determined as 482.35 m^2/g. Pore size distribution curve, calculated from Barrett-Joyner-Halenda analysis, showed that the pore width of **TAPB-TP-PA-COF** is centered at 3.0 nm, which is in good agreement with their simulated structure. d) ^{13}C (CP/MAS) NMR spectrum. The peaks at 109-160 ppm and 167 ppm are respectively associated with aromatic and carboxylic acid carbons, the asterisks denote the solvent *n*-butyl alcohol. e) TEM image of **TAPB-TP-PA-COF**. f) SEM image of **TAPB-TP-PA-COF**.

The simulation method is the same as that of **TAPB-DMTP-PA-COF**. Atomistic coordinates for the AA-stacking mode of **TAPB-TP-PA-COF** (space group *P*6, $a = b = 37.2693$ Å, $c = 3.6909$ Å, $\alpha = \beta = 90°$ and $\gamma = 120°$, w*R*p = 2.94 % and *R*p = 2.15 %).

Table S5. Simulated structure of **TAPB-TP-PA-COF**

Atom	x/a	y/b	z/c	Atom	x/a	y/b	z/c
C1	0.35768	0.64720	0.65761	C2	0.37649	0.69064	0.65769
C3	0.38333	0.62655	0.66159	C4	0.36817	0.58687	0.50826

C5	0.39095	0.56602	0.52823	C6	0.43154	0.58758	0.67159
C7	0.44717	0.62721	0.81604	C8	0.42304	0.64612	0.81957
N9	0.45579	0.56999	0.66988	C10	0.44274	0.53146	0.53606
C11	0.47174	0.51495	0.53913	C12	0.45740	0.47214	0.54528
C13	0.48530	0.45745	0.54351	H14	0.40984	0.70916	0.65909
H15	0.33970	0.57351	0.35669	C16	0.37560	0.52494	0.39968
H17	0.47790	0.64316	0.93382	H18	0.43556	0.67586	0.95216
C19	0.40237	0.50853	0.39755	H20	0.47311	0.42429	0.54410
H21	0.39154	0.47791	0.28763	C22	0.66816	0.50271	0.28589
O23	0.67660	0.53136	0.07857	O24	0.70015	0.49815	0.43288
H25	0.72843	0.51941	0.33727	H26	0.42468	0.44973	0.55715

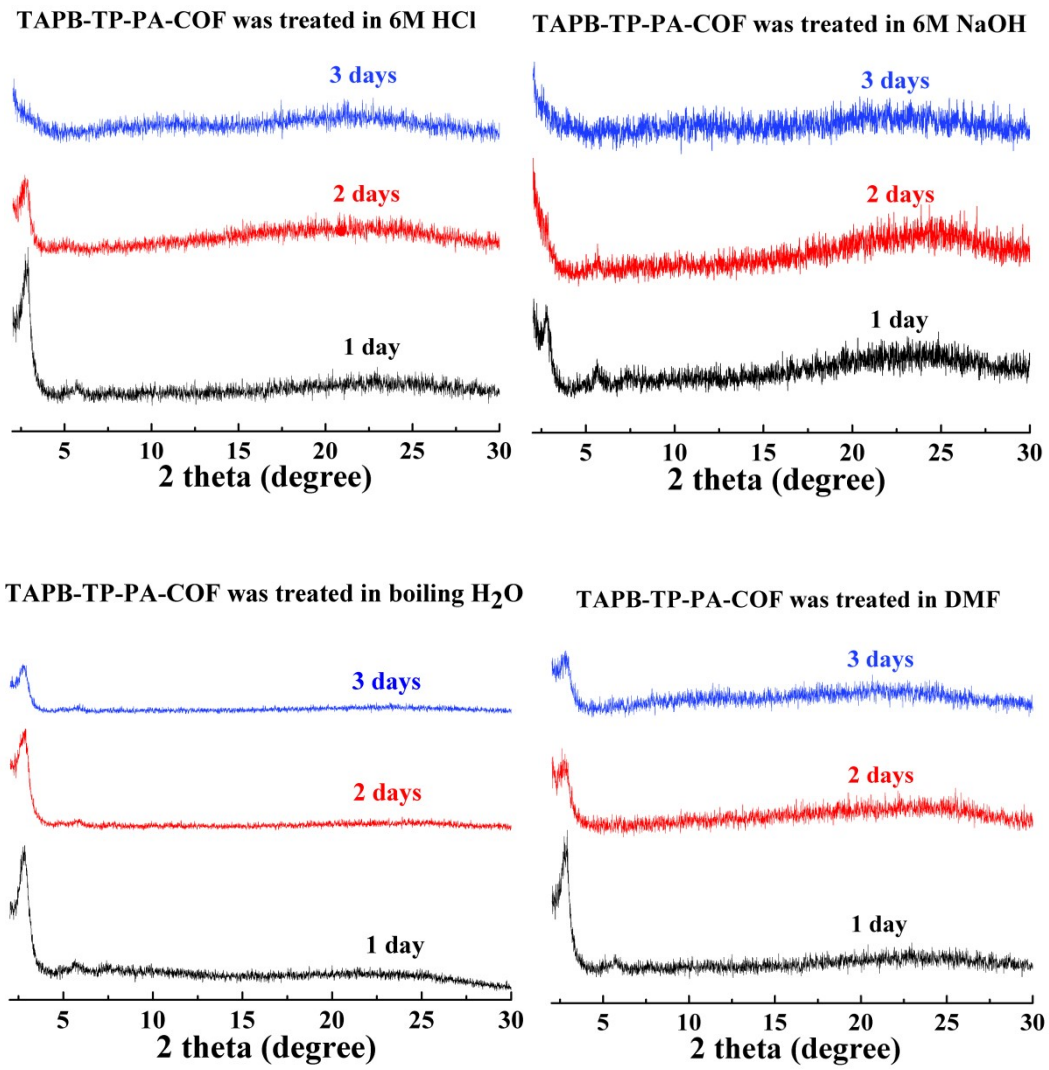

Fig. S23 PXRD patterns of **TAPB-TP-PA-COF** treated in different solvents. No obvious weight loss for **TAPB-TP-PA-COF** treated in boiling H_2O and 6M NaOH was observed, but there is about 7.3 % weight loss in DMF and 6M HCl after treatment.

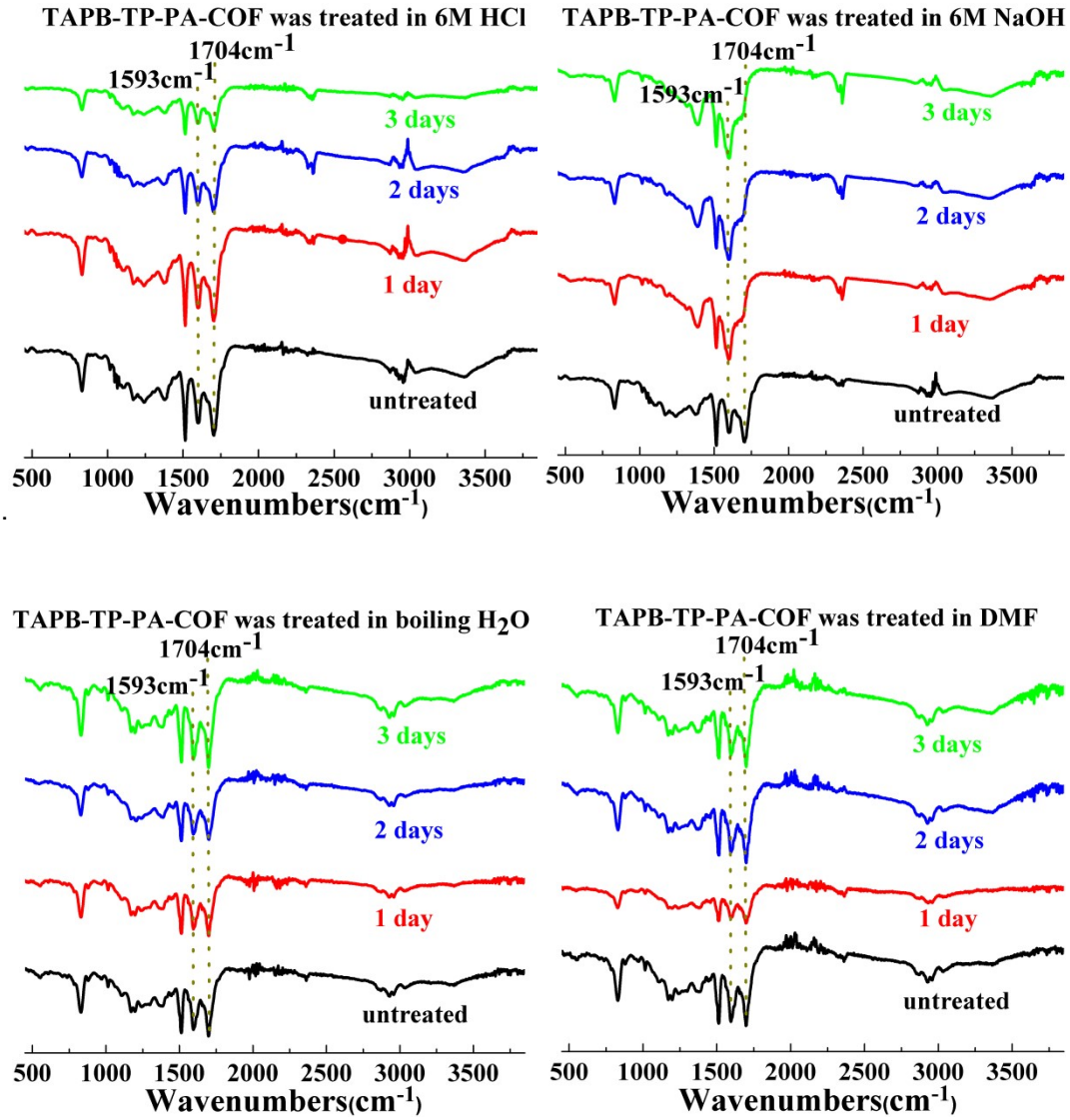

Fig. S24 FT-IR spectra of **TAPB-TP-PA-COF** treated in different solvents.

5. Synthesis and characterization of TAPT-TP-PA-COF

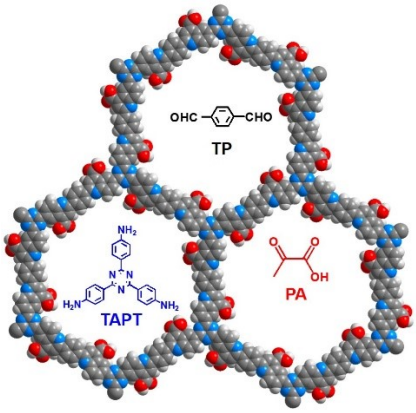

TAPT-TP-PA-COF

TAPT-TP-PA-COF was obtained by combination of TATP, TFPB and PA via Doebner reaction. The synthesis procedure is the same as that of **TAPB-DMTP-PA-COF**. Yield, 87 %.

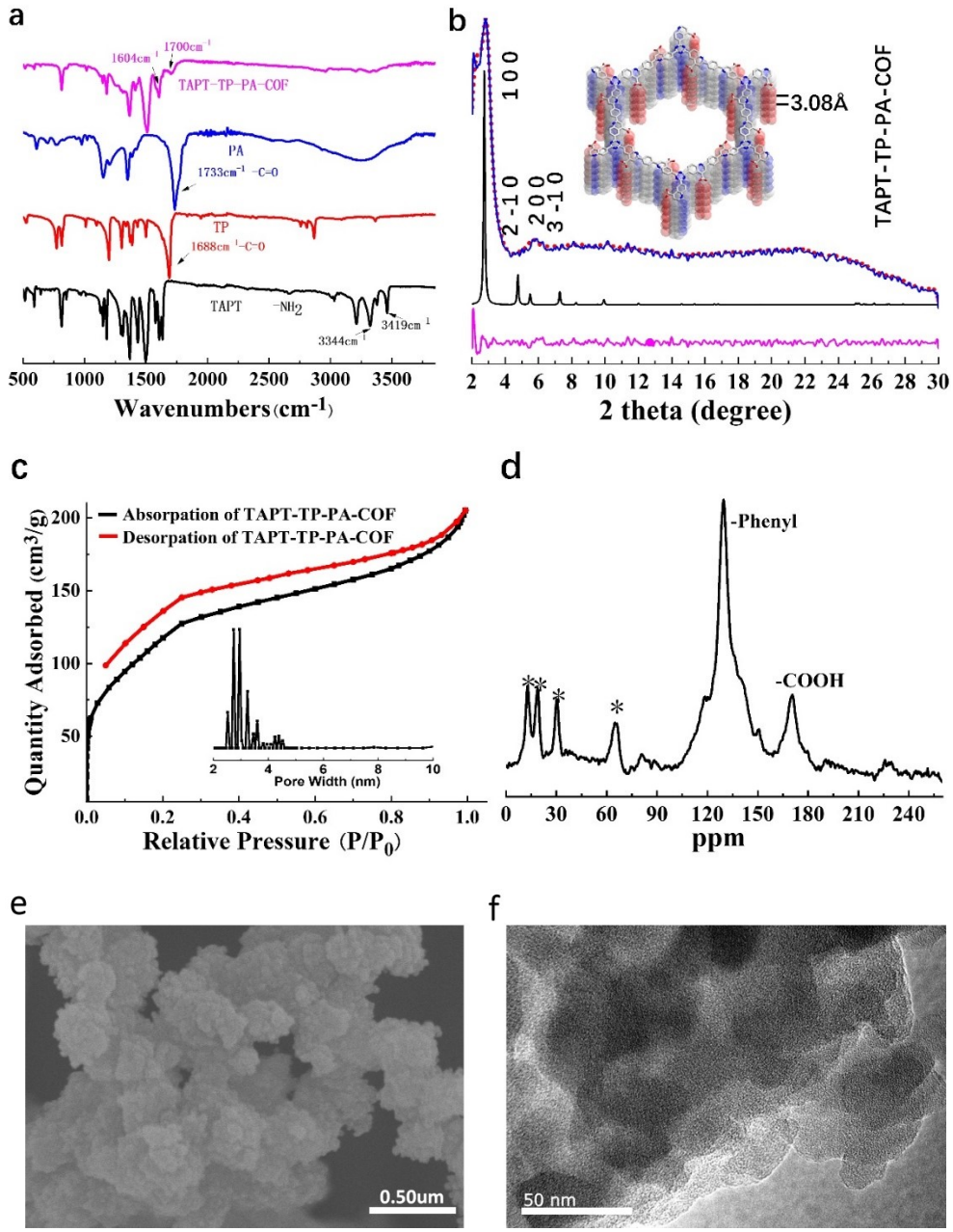

Fig. S25 a) FT-IR spectra of **TAPT-TP-PA-COF** and its monomers. The characteristic peaks of amine (3344 and 3419 cm^{-1}), aldehyde (1688 cm^{-1}) and C=O of pyruvic acid (1733 cm^{-1}) in the monomers disappeared after reaction, meanwhile the characteristic peaks at 1604 and 1700 cm^{-1} appeared, demonstrating the formation of **TAPT-TP-PA-COF**. b) PXRD of **TAPT-TP-PA-COF**: comparison between the experimental (blue line) and Pawley refined (red dots) profiles, the simulated patterns for eclipsed (AA) stacking mode (black line) and the refinement difference (purple line). Inset is simulated structure of **TAPT-TP-PA-COF**. c) N_2 adsorption at 77 K revealed absorption amount of **TAPT-TP-PA-COF** is 205.22 cm^3/g, and its surface area calculated on basis of the BET model was determined as 438.33 m^2/g. Pore size distribution curve, calculated from Barrett-Joyner-Halenda analysis, showed that the pore width of **TAPT-TP-PA-COF** is centered at 3.1 nm, which is in good agreement with their simulated structure. d) ^{13}C (CP/MAS) NMR spectrum. The peaks at 109-160 ppm and 170 ppm are respectively associated with aromatic and carboxylic acid carbons, the asterisks denote the solvent *n*-butyl alcohol. e) TEM image of **TAPT-TP-PA-COF**. f) SEM image of **TAPT-TP-PA-COF**.

The simulation method is the same as that of **TAPB-DMTP-PA-COF**. Atomistic coordinates for the AA-stacking mode of **TAPT-TP-PA-COF** (space group *P*6, $a = b = 37.0544$ Å, $c = 3.5489$ Å, $\alpha = \beta = 90°$ and $\gamma = 120°$, w*R*p = 2.99 % and *R*p = 2.15 %).

Table S6. Simulated structure of **TAPT-TP-PA-COF**

Atom	x/a	y/b	z/c	Atom	x/a	y/b	z/c
C1	0.35693	0.64802	0.59364	N2	0.37532	0.69011	0.59410
C3	0.38260	0.62762	0.60311	C4	0.36479	0.58506	0.51447
C5	0.38841	0.56475	0.53588	C6	0.43104	0.58876	0.63521
C7	0.44878	0.63104	0.71917	C8	0.42484	0.65043	0.70415
N9	0.45548	0.57116	0.64521	C10	0.44116	0.53050	0.56026
C11	0.47084	0.51430	0.57007	C12	0.45729	0.47137	0.57874
C13	0.48604	0.45741	0.57543	H14	0.33289	0.56893	0.41893
C15	0.37200	0.52181	0.45195	H16	0.48134	0.64880	0.79745
H17	0.43918	0.68325	0.77474	C18	0.39917	0.50551	0.45835
H19	0.47448	0.42416	0.57603	H20	0.38709	0.47332	0.38052
C21	0.67269	0.50751	0.35995	O22	0.68207	0.53884	0.17705
O23	0.70441	0.50115	0.49133	H24	0.73230	0.52518	0.40948
H25	0.42463	0.44817	0.59261				

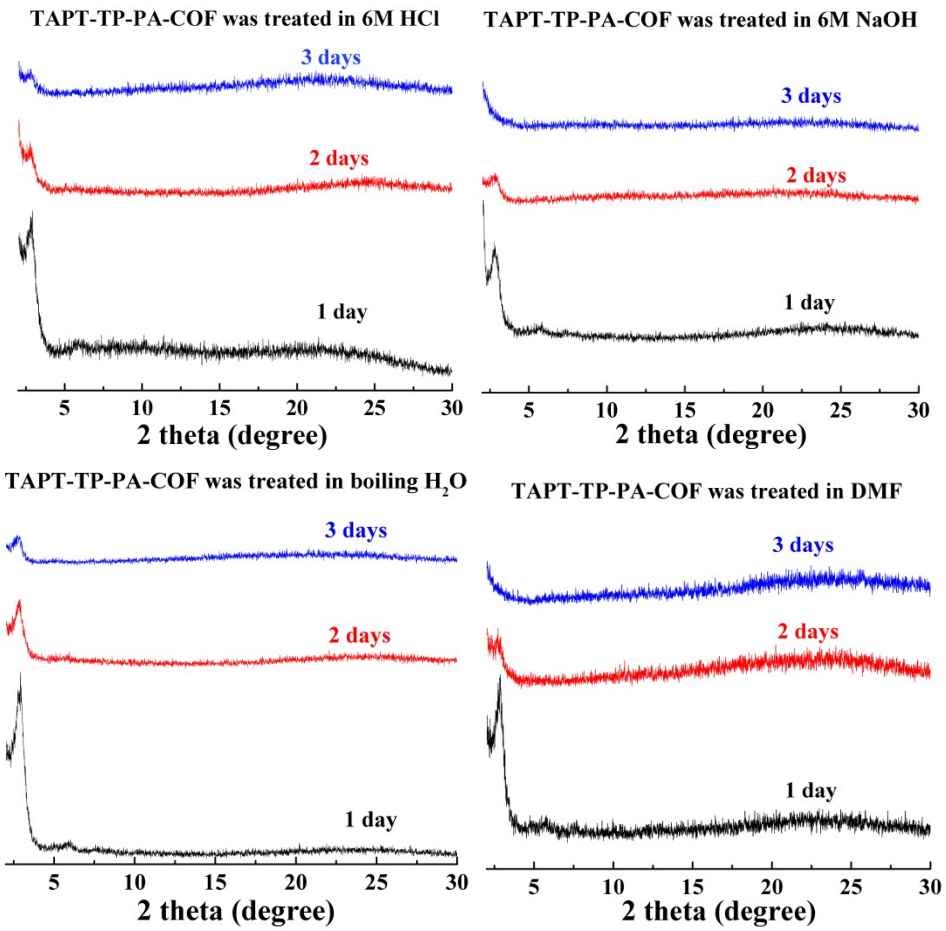

Fig. S26 PXRD patterns of **TAPT-TP-PA-COF** treated in different solvents. No obvious weight loss for **TAPT-TP-PA-COF** treated by boiling H_2O and 6M NaOH was observed, but there is about 6.3 % weight loss in DMF and 6M HCl after treatment.

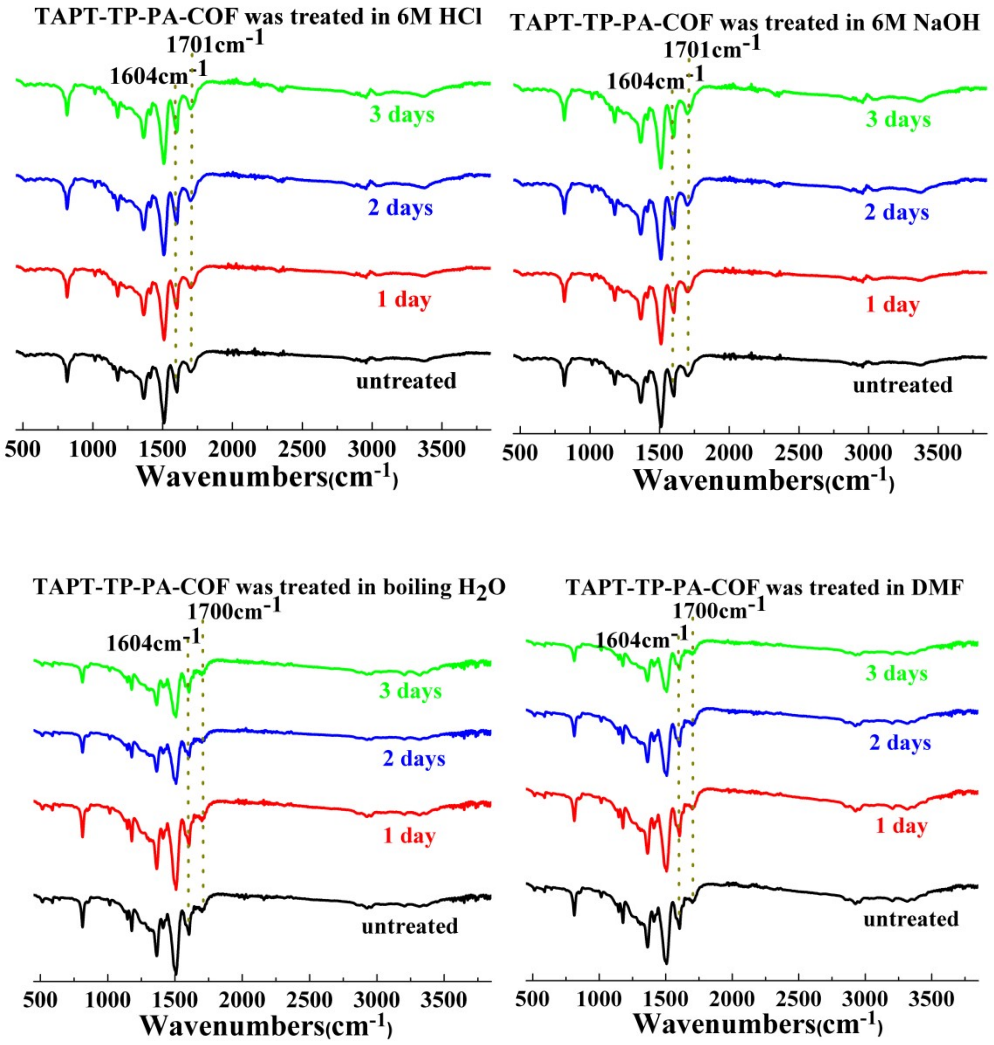

Fig. S27 FT-IR spectra of **TAPT-TP-PA-COF** treated in different solvents.

IV. Synthesis and characterization of benzylidenemalononitrile

A mixture of benzaldehyde dimethyl acetal (1.5 mL, 10.0 mmol), malononitrile (0.72g, 11.0 mmol), and **TAPB-DMTP-PA-COF** (30 mg, 3 mol %) was stirred for 5 h at 75°C in air to afford the corresponding benzylidenemalononitrile.

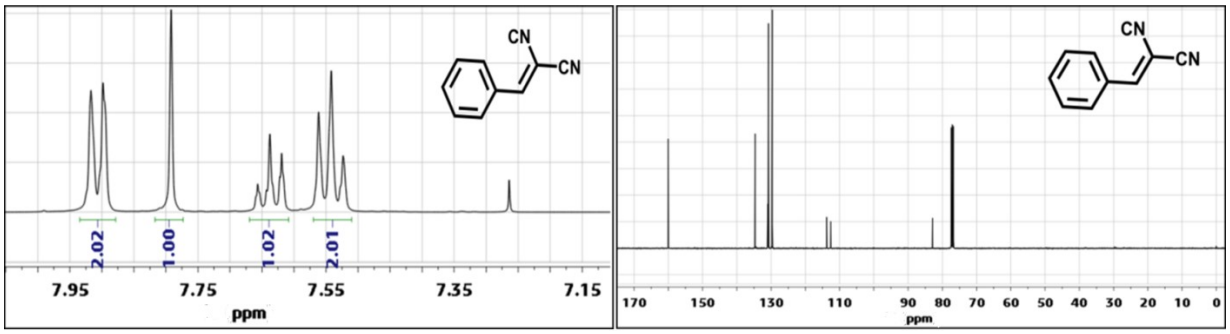

Fig. S28 ^{1}H NMR and ^{13}C NMR spectra (400 MHz, $CDCl_3$) of benzylidenemalononitrile.

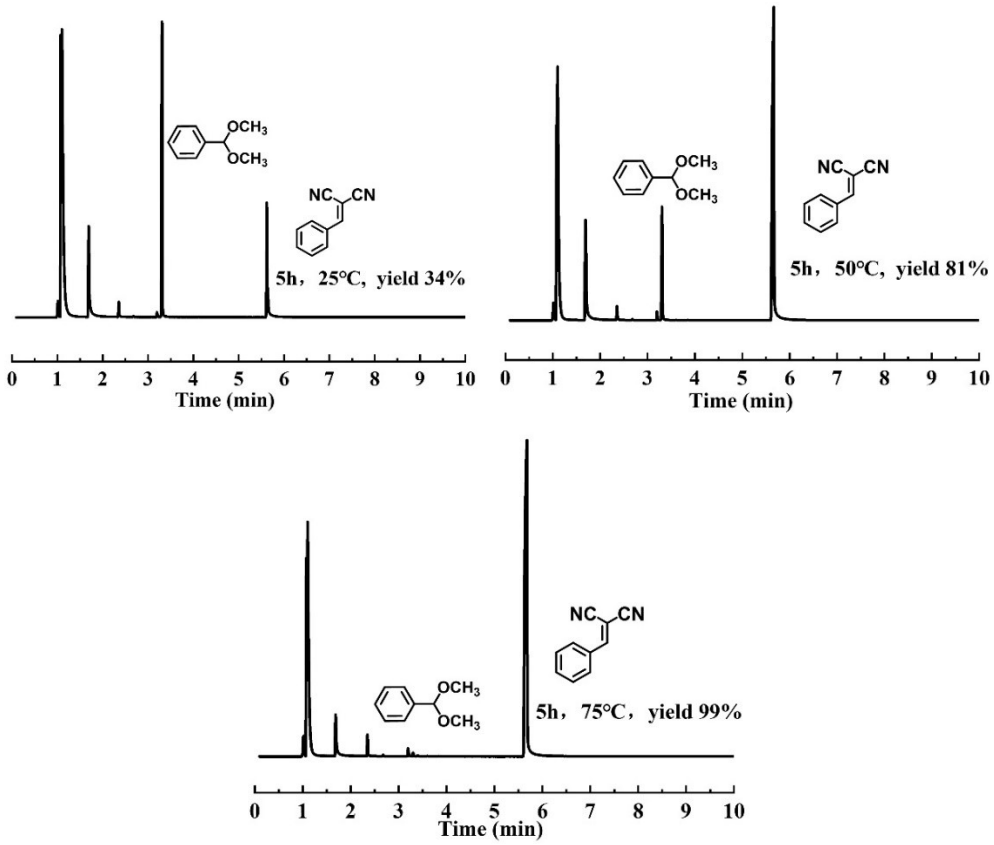

Fig. S29 GC analysis of the **TAPB-DMTP-PA-COF**-catalysed deacetalization−Knoevenagel condensation at difference temperature: the relationship between time and yield.

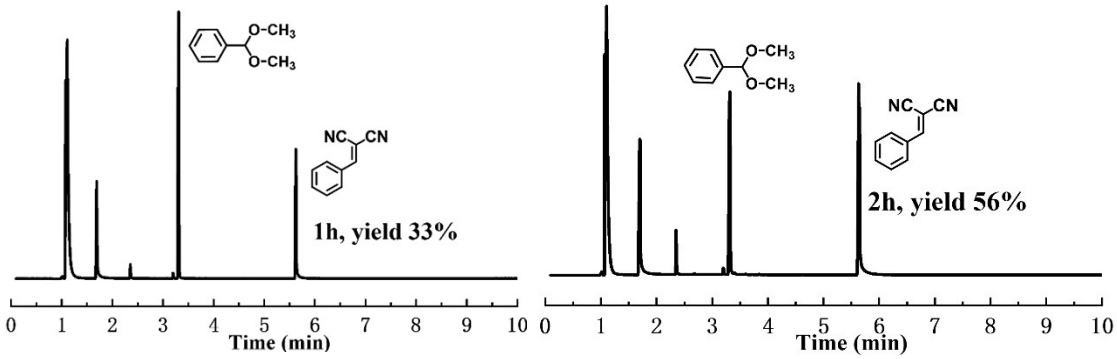

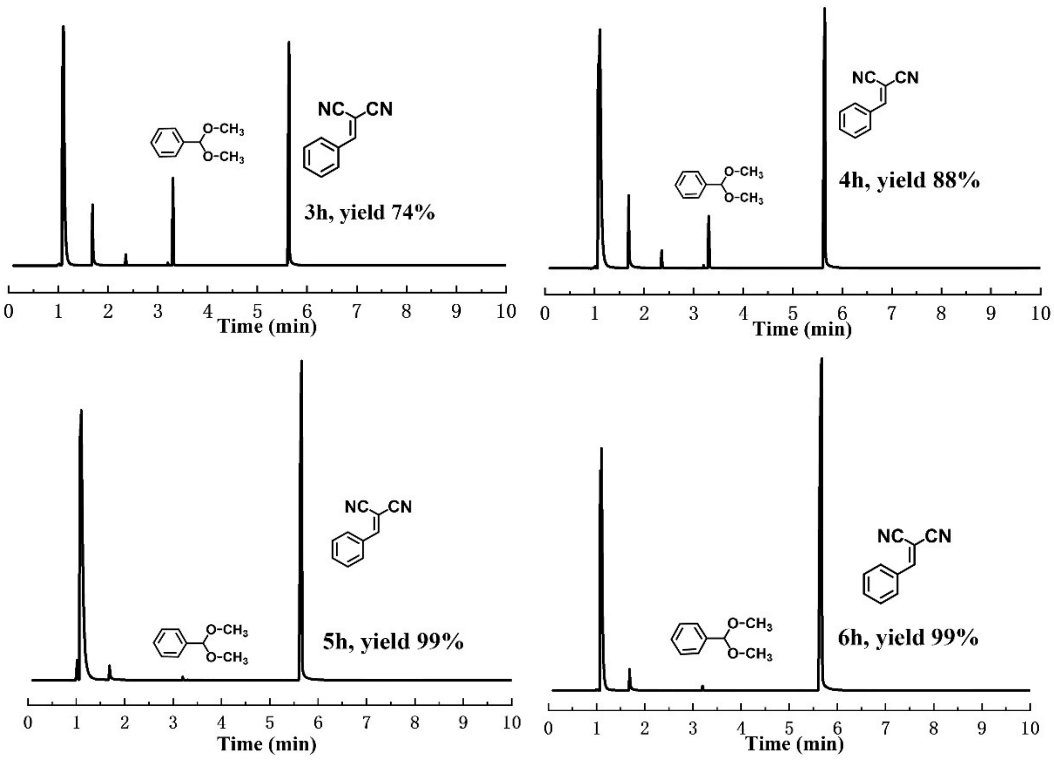

Fig. S30 GC analysis of the **TAPB-DMTP-PA-COF**-catalysed deacetalization−Knoevenagel condensation: the relationship between time and yield.

V. Leaching test

The solid catalyst **TAPB-DMTP-PA-COF** was isolated from the hot reaction solution after reaction ignition for 2 h, whereas the filtrate was transferred to a new vial and the reaction was carried out under the same conditions for additional 4 h under the same conditions. No significant conversion for the product was detected.

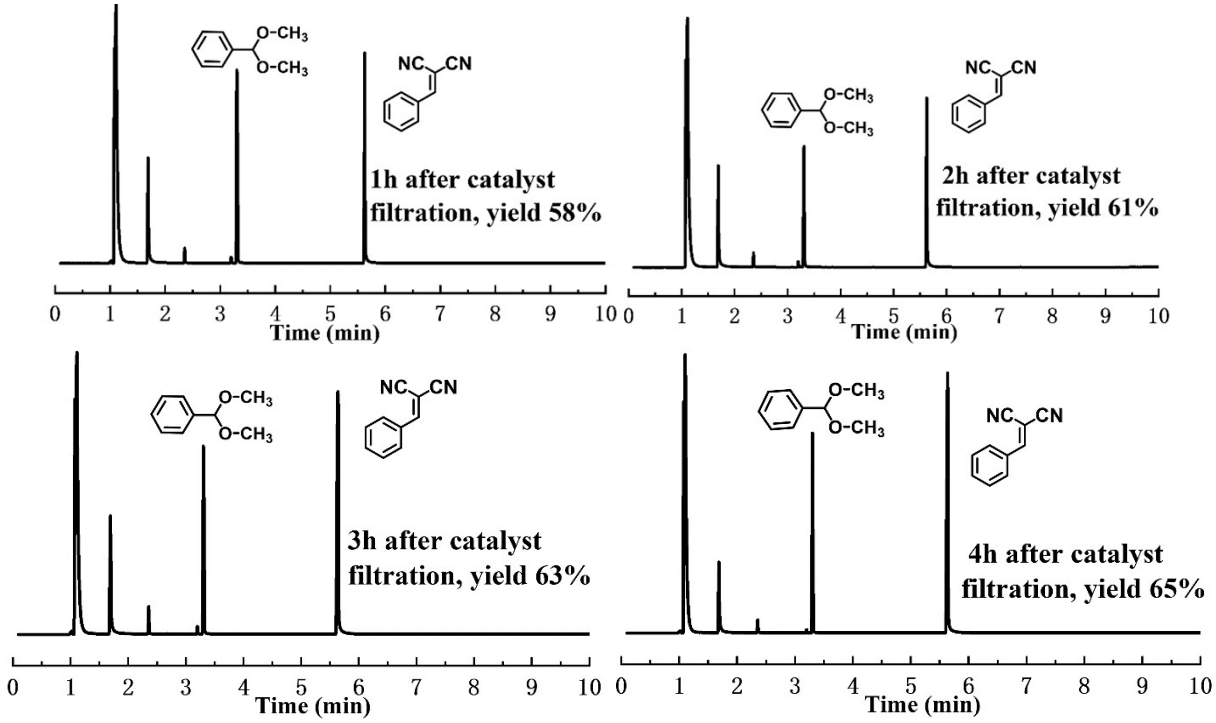

Fig. S31 The GC analysis after removing the COF catalyst.

VI. Catalyst regeneration

After reaction, **TAPB-DMTP-PA-COF** was recovered by centrifugation, then washed with ethanol (3.0 mL) and dichloromethane (3.0 mL) (3 times), and dried at 90 °C in vacuum for the next run under the same reaction conditions.

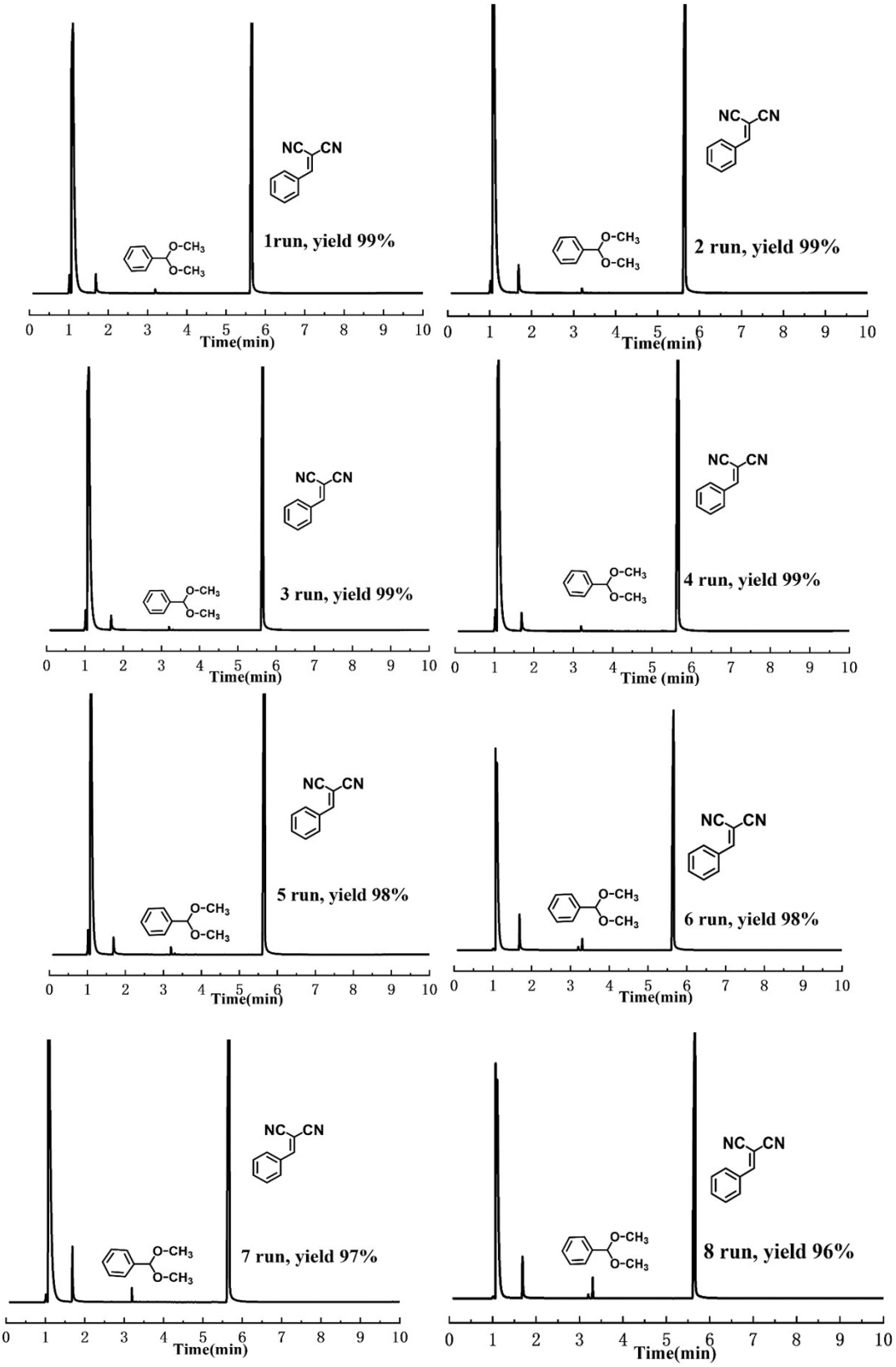

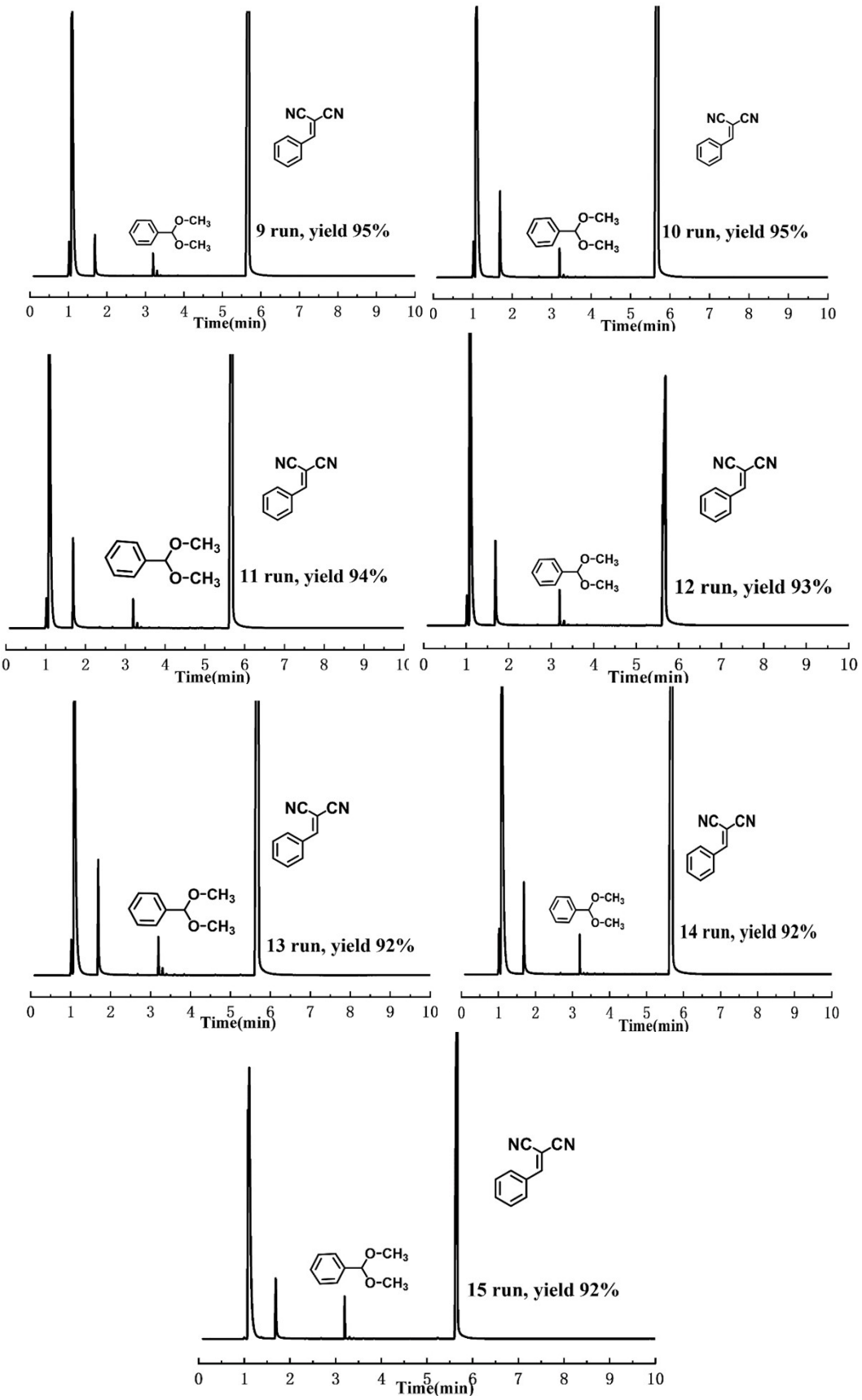

Fig. S32. GC results of the **TAPB-DMTP-PA-COF**-catalysed deacetalization−Knoevenagel condensation for fifteen runs.

VII. Comparison of TAPB-DMTP-PA-COF with the reported catalysts

Table S7. Comparison of **TAPB-DMTP-PA-COF** with the reported catalysts for one-pot cascade deacetalization−Knoevenagel condensation.

catalyst	conditions	recycle	yield	ref.
MCM-41-P1	MeCN, toluene / 80 °C / 5h	3	90	1
HisAA-220	MeCN / 80 °C / 4h	5	77	2
MIL-101(Cr)@CS	MeCN / 80 °C / 12 h	5	99	3
Pd@N-ZDC@PTA-mSiO_2	DMF / 80 °C / 24 h	5	>99	4
$[Zn_2(L)_2(H_2O)_4]\cdot 2(H_2O)\cdot 6(DMF)$	DMF / 80 °C / 3h	5	93.5	5
PCN-905-SO_2	Toluene / 90 °C / 1 h.	0	95.5	6
Zr_{12} BDC-NH_2	$CDCl_3$ / 55 °C / 24 h.	3	91.8	7
PCN-222-Co@TpPa-1	DMSO-d_6 / 50 °C / 10 h.	5	99.3	8
Yb-BDC-NH_2	DMSO-d_6 / 50 °C / 24 h	4	97	9
$[Zn_{24}(BDPO)_{12}(DMF)_{12}]\cdot 6DMF\cdot 52H_2O$	Toluene / 90 °C / 3 h	5	99	10
BNP-2.1	Toluene / 80 °C / 24 h	4	98.5	11
3D DL-COF-1	$CDCl_3$ / r t / 20 h	3	98	12
MIL-101-AB-0.32	DMF, 1,2,4-trichlorobenzene/ 363 K	3	99	13
Pickering Emulsion Droplets	Water, toluene / 60 °C /19 h	4	75	14
2,3-DhaTph	Toluene / 80 °C / 1h	5	96	15
PPAF-SO3H-NH_2	Toluene / 90°C / 1 h	7	87	16
LZSM-5-AT−OH^-	MeCN / 353 K / 15 h	10	91.2	17
PPAF-SO_3H-NH_2	Toluene / 90 °C / 1 h	8	100	18
SAB	Ethyl acetate / 50°C / 12 h	4	99	19
Ti^{4+}-mont/HT	Toluene / 80 °C / 1 h	0	93	20
TAPB-DMTP-PA-COF	**Solvent-free, 75°C, 5h**	**15**	**99**	**this work**

VIII. Control experiments for clarifying the cascade deacetalization−Knoevenagel condensation reaction process

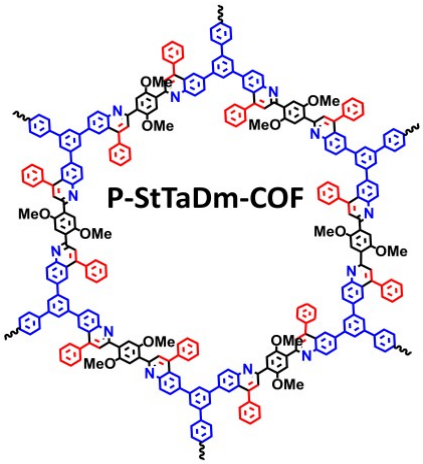

Fig. S33 Structure of P-StTaDm-COF.[21]

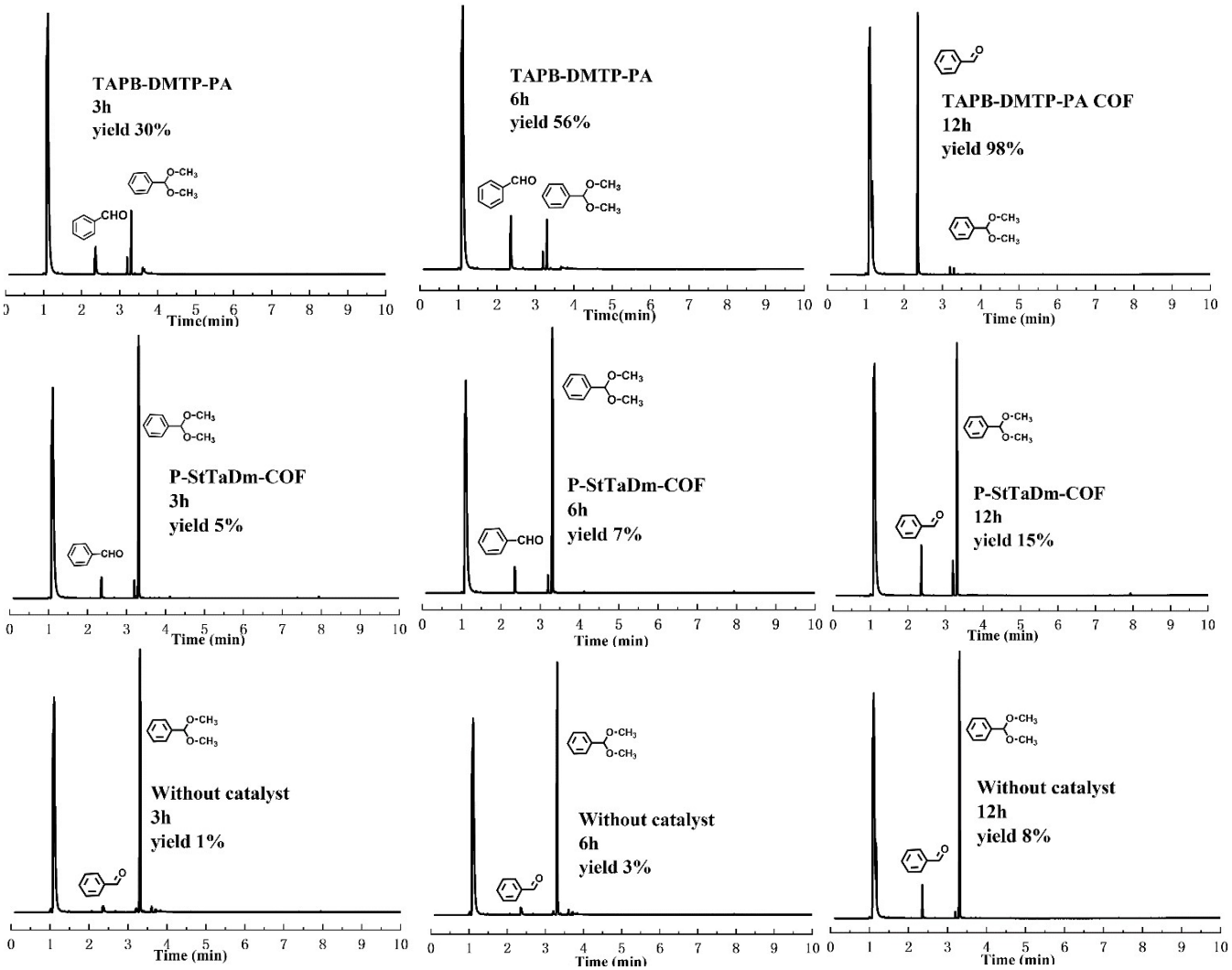

Fig. S34 GC results of the deacetalization catalysed by **TAPB-DMTP-PA-COF**, P-StTaDm-COF and without catalyst.

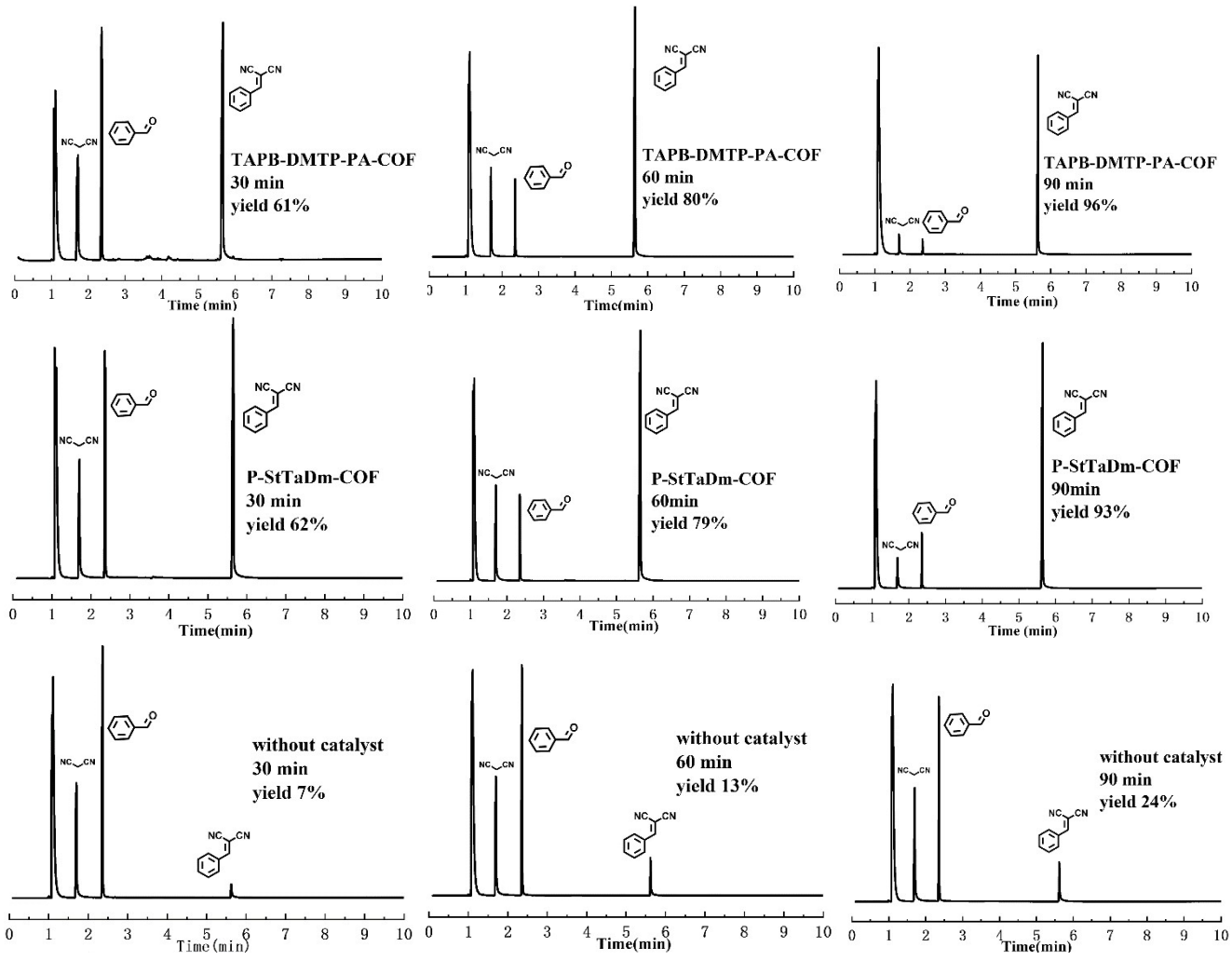

Fig. S35 GC results of the Knoevenagel condensation by **TAPB-DMTP-PA-COF**, P-StTaDm-COF and without catalyst.

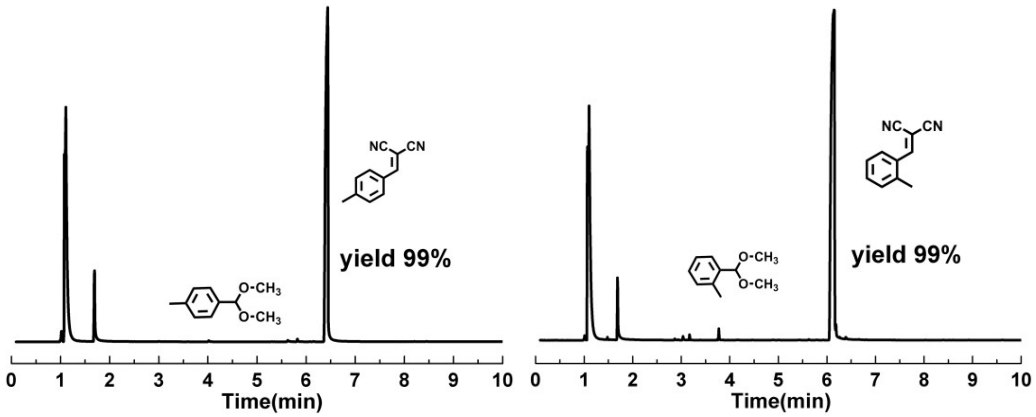

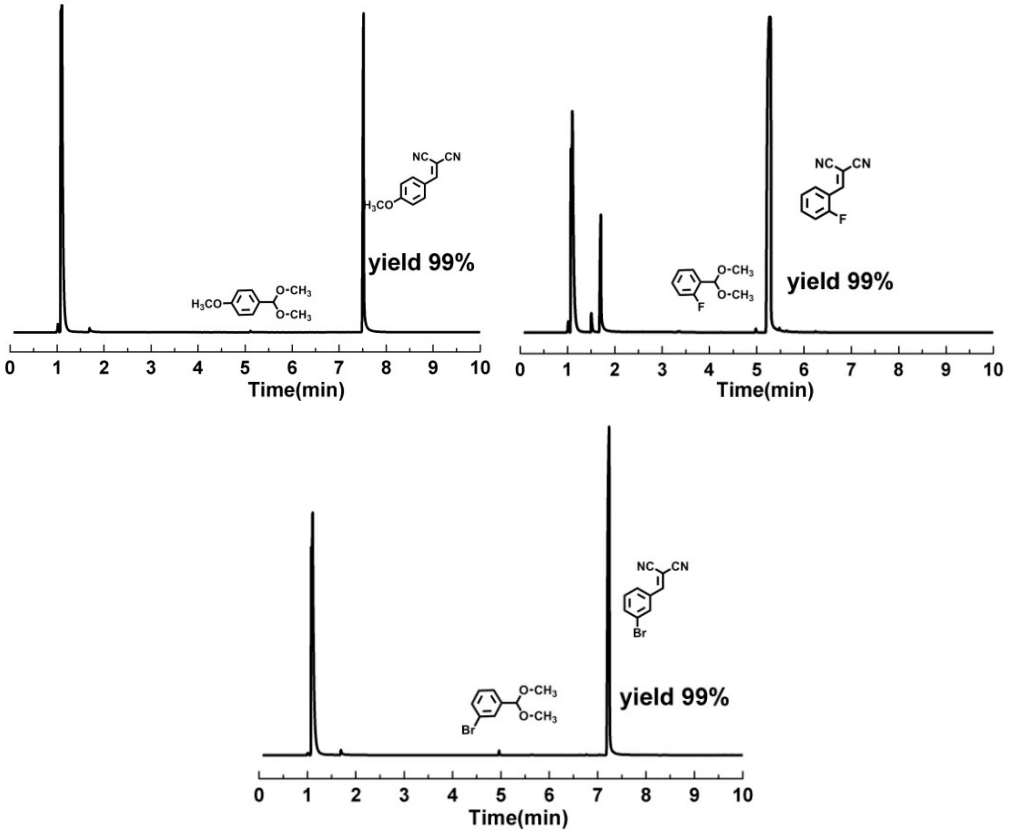

Fig. S36 GC analysis for the scope of **TAPB-DMTP-PA-COF**-catalysed one-pot tandem deacetalization-Knoevenagel condensation reactions.

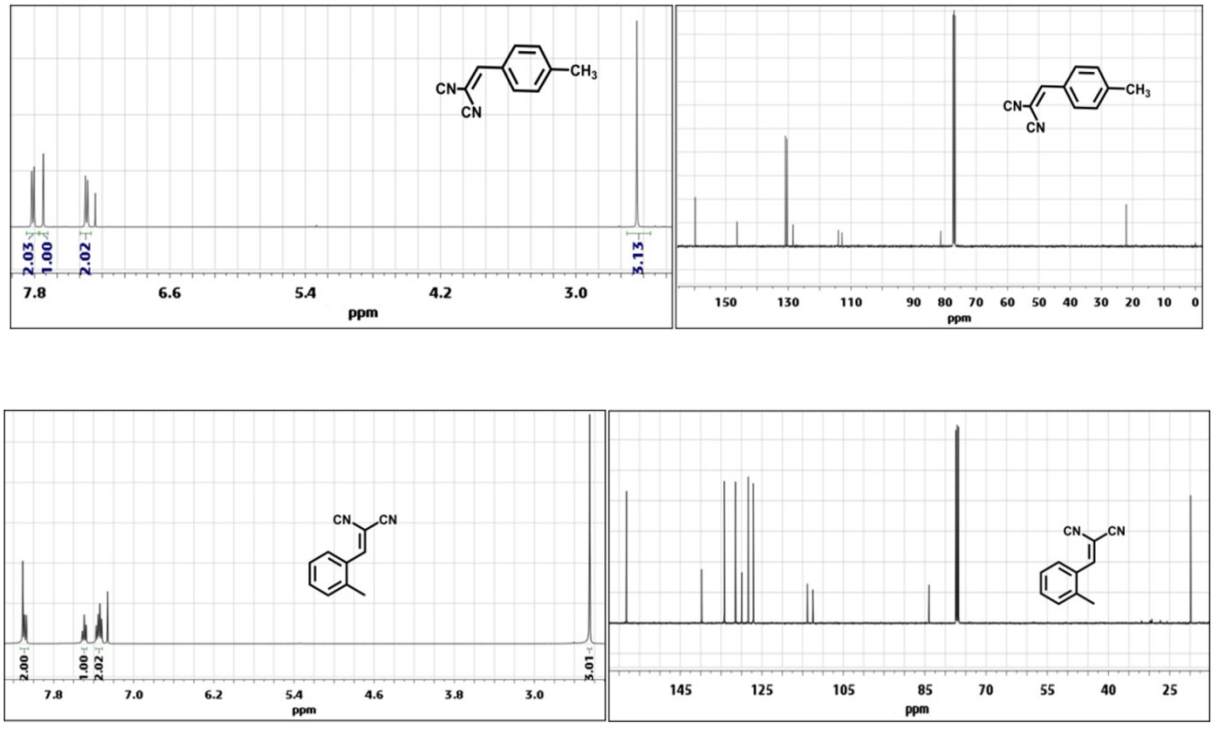

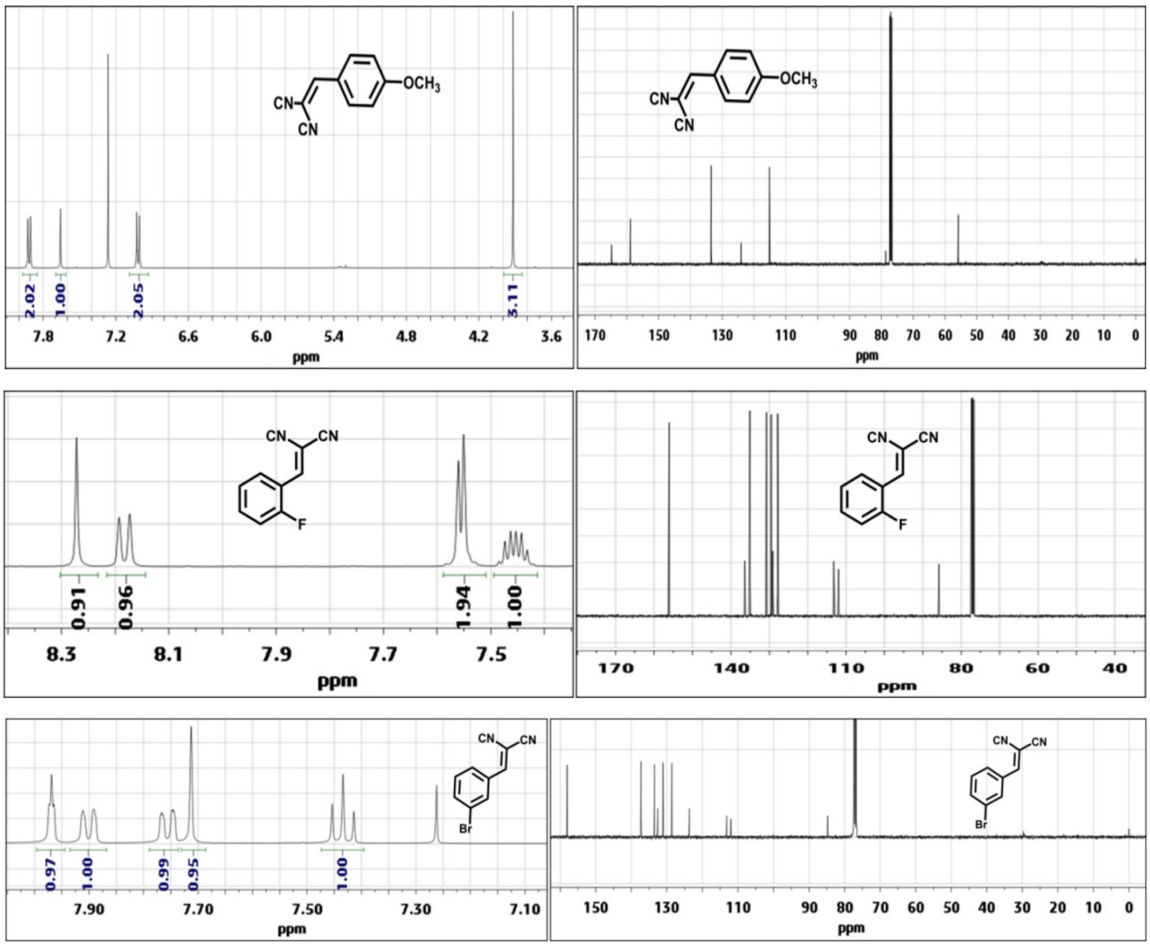

Fig. S37 ^{1}H NMR and ^{13}C NMR spectra (400 MHz, $CDCl_3$) of substituted benzylidenemalononitriles (for Fig. 4).

IX. Continuous flow-through operation

A mixture of benzaldehyde dimethylacetal (1.5 mL, 10.0 mmol), H_2O (5 mL), malononitrile (0.80 g, 12.0 mmol) in C_2H_5OH solution (40 mL) was pumped through the spiral transparent glass tube which is evenly charged with a mixture of **TAPB-DMTP-PA-COF** (0.4 g) and glass microsphere (8.5 g) at 75 °C with a flow rate of 5 mL min^{-1}.

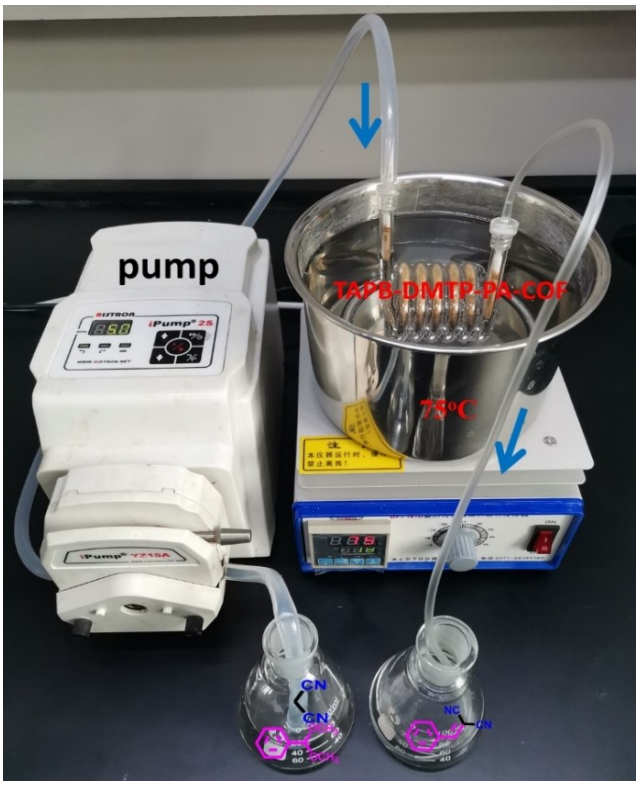

Fig. S38 Photograph of the continuous-flow reactor for the synthesis of benzylidenemalononitrile at gram-level.

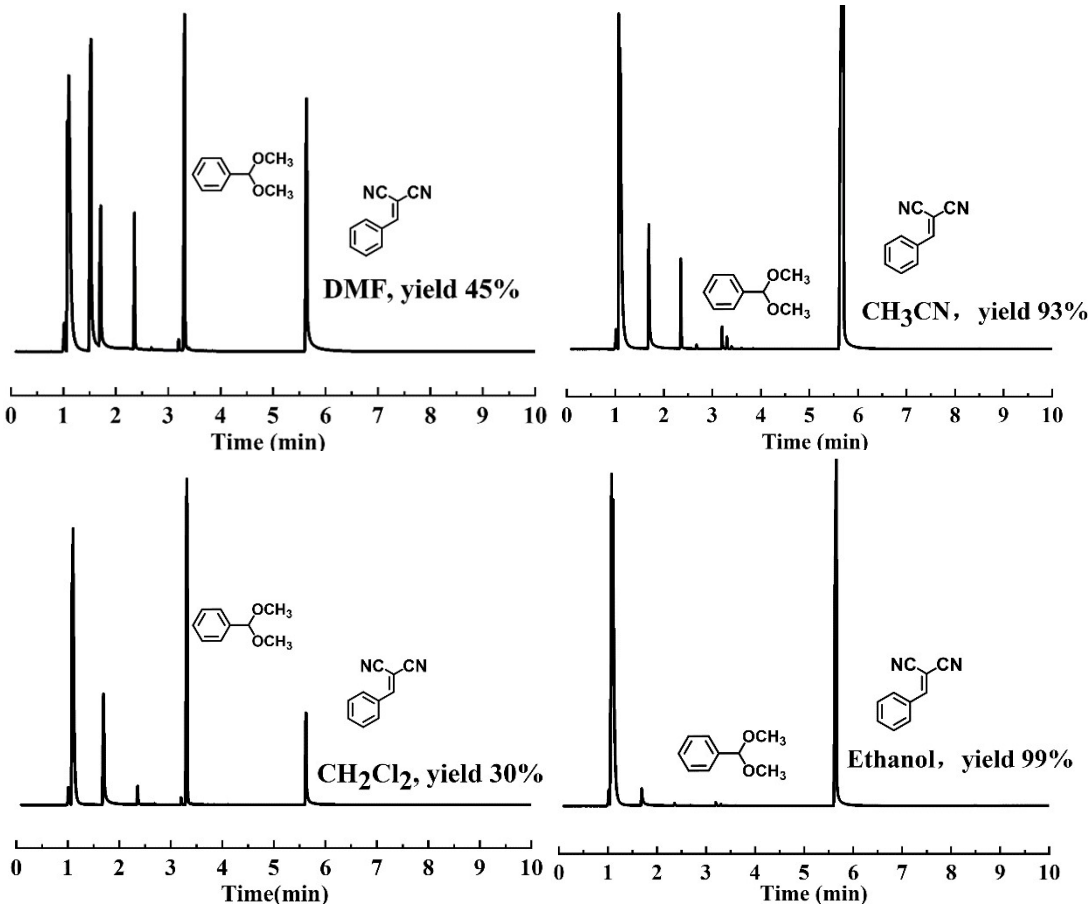

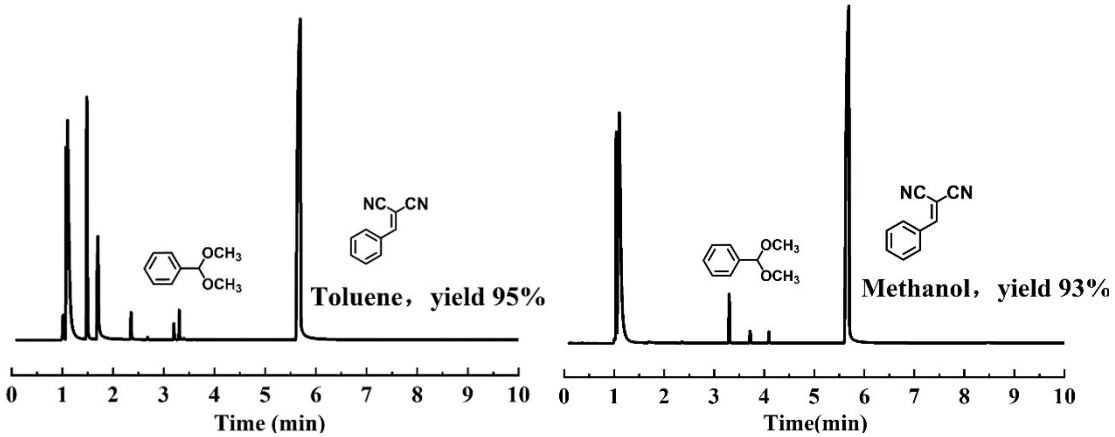

Fig. S39 Optimization of the model reaction perfomed on COF-based tubular reactor in various solvents at 75 °C.

X. Reference

1. J. W. Cleveland, D. R. Kumar, J. Cho, S. S. Jang, C, W. Jones, *Catal. Sci. Technol*., 2021, **11**, 1311-1322.

2. S. Rat, A. Chavez-Sanchez, M. Jerigová, D. Cruz, M. Antonietti, *ACS Appl. Polym. Mater*., 2021, **3**, 2588-2597.

3. Z. S. Zhao, Y. Zhang, T. Fang, Z. B. Han, F. S. Liang, *ACS Appl. Nano Mater*., 2020, **3**, 6316-6320.

4. J. Wu, G. G. Chang, Y. Q. Peng, X. C. Ma, S. C. Ke, S. M. Wu, Y. X. Xiao, G. Tian, T. Xia, X. Y. Yang, *Chem. Commun*., 2020, **56**, 6297-6300.

5. A. Karmakar, M. M. A. Soliman, G. M. D. M. Rúbio, M. F.C. G. Silva, A. J. L. Pombeiro, *Dalton Trans*., 2020, **49**, 8075-8085.

6. L. Feng, Y. Wang, K. Zhang, K. Y. Wang, W. Fan, X. Wang, J. A. Powell, B. Guo, F. Dai, L. Zhang, R. Wang, D. Sun, H. C. Zhou, *Angew. Chem. Int. Ed*., 2019, **58**, 16682-16690.

7. S. B. Peh, Y. Cheng, J. Zhang, Y. Wang, G. H. Chan, J. Wang, D. Zhao, *Dalton Trans*., 2019, **48**, 7069-7073.

8. M. L. Gao, M. H. Qi, L. Liu, Z. B. Han, *Chem. Commun*., 2019, **55**, 6377-6380.

9. Y. Zhang, Y. Wang, L. Liu, N. Wei, M. L. Gao, D. Zhao, Z. B. Han, *Inorg. Chem*. 2018, **57**, 2193-2198.

10. H. He, D. Y. Zhang, F. Guo, F. Sun, *Inorg. Chem*., 2018, **57**, 7314-7320.

11. J. Zhao, B.Lin, Y. Zhu, Y. Zhou, H. Liu, *Catal. Sci. Technol*. 2018, **8**, 5900-5905.

12. H. Li, Q. Pan, Y. Ma, X. Guan, M. Xue, Q. Fang, Y. Yan, V. Valtchev, S. Qiu, *J. Am. Chem. Soc*., 2016, **138**, 14783-14788.

13. B. Li, D. Ma, Y. Li, Y. Zhang, G. Li, Z. Shi, S. Feng, M. J. Zaworotko, S. Ma, *Chem. Mater*., 2016, **28**, 4781-4786.

14. H. Yang, L. Fu, L. Wei, J. Liang, B. P. Binks, *J. Am. Chem. Soc.,* 2015, **137**, 1362-1371.

15. D. B. Shinde, S. Kandambeth, P. Pachfule, R. R. Kumar, R. Banerjee, *Chem. Commun*., 2015, **51**, 310-313.

16. E. Merino, E. Verde-Sesto, E. M. Maya, A. Corma, M. Iglesias, F. Sánchez, *Appl. Catal. A: Gen*., 2014, **469**, 206-212.

17. L. Xu, C. Li, K. Zhang, P. Wu, *ACS Catal*., 2014, **4**, 2959-2968.
18. E. Merino, E. Verde-Sesto, E. M. Maya, M. Iglesias, F. Sánchez, A. Corma, *Chem. Mater.*, 2013, **25**, 981-988.
19. N. R. Shiju, A. H. Alberts, S. Khalid, D. R. Brown, G. Rothenberg, *Angew. Chem. Int. Ed.*, 2011, **50**, 9615-9619.
20. K. Motokura, N. Fujita, K. Mori, T. Mizugaki, K. Ebitani, K. Kaneda, *J. Am. Chem. Soc.,* 2005, **127**, 9674-9675.
21. X.-T. Li, J. Zou, T.-H. Wang, H.-C. Ma, G.-J. Chen and Y.-B. Dong, *J. Am. Chem. Soc.*, 2020, **142**, 6521-6526